ALPINE GLACIAL GEOMORPHOLOGICAL STUDIES IN THE CENTRAL ANDES USING LANDSAT THEMATIC MAPPER IMAGES

Andrew G. Klein,[1,2] and Bryan L. Isacks[1]

[1]Department of Geological Sciences, Snee Hall, Cornell University,
Ithaca, NY 14853

[2]current affiliation and address:
Universities Space Research Association, Seabrook, MD 20706
NASA/Goddard Space Flight Center
Mail Code 974
Greenbelt, MD 20771
aklein@glacier.gsfc.nasa.gov

Table of Contents

Extended Abstract

Satellite images are a powerful tool for geomorphological studies, but have been used far less than aerial photography. In particular, the regional overview provided by Landsat Thematic Mapper (TM) images has been found to be extremely valuable for studying late Pleistocene glaciation in the central Andes. Standard image processing techniques were used to create a Landsat Thematic Mapper (TM) mosaic of the central Andes suitable for a variety of geomorphological studies. The mosaic was used to map the extent of late Pleistocene glaciation from the extent of well-preserved terminal moraines and other glacial geomorphological features. Moraines in many portions of the central Andes are unusually well preserved due to the region's semiarid to arid environment.

Late Pleistocene glaciers were more numerous and larger than their modern counterparts. In late Pleistocene times, approximately 11,000 glaciers existed in the central Andes. This represents a 7 fold increase over the approximately 1500 glaciers that exist in the region today. At their maximum, late Pleistocene palaeo-glaciers in this region covered approximately 29,800 km^2 which dwarfs the present area covered by glaciers and snowcover. Estimates of present glacier extent in the region range from 700 km^2 to 1300 km^2. The lower estimated is based on incomplete glacier inventory data while the higher number includes both glaciers and snow cover classified on Landsat TM images.

Using a scaling relationship between glacier area and volume, the ice volumes of both late Pleistocene and modern glaciers in the central Andes were estimated. The total volume of the region's palaeo-glaciers is estimated to be 3700

km^3. The modern total is estimated to be only one percent of this volume or approximately 35-53 km^3.

Using the "toe-to-headwall altitude ratio" (THAR) method, the equilibrium line altitude (ELA) of each palaeo-glacier was calculated. This allowed the magnitude and pattern of ELA (snowline) depression to be calculated with a level of detail not previously possible. Modern and late Pleistocene ELAs exhibit a similar northeast to southwest rise in elevation that is a response to decreasing precipitation across the region. The pattern of ELA depression was found to vary considerably from the uniform 1000 m lowering often assumed for tropical latitudes. In particular, the presence of the high Altiplano plateau imposes a non-climatic constraint on glacial expansion and snowline lowering.

Short Abstract

A mosaic of Landsat Thematic Mapper images was constructed to enable the extent of late Pleistocene glaciation in the central Andes between 15 and 22° S latitude to be mapped. From the mapping, the number, area, and volume of the late Pleistocene glaciers were calculated and the magnitude and pattern of late Pleistocene snowline depression was estimated.

Keywords

remote sensing, snowline, Andes

Introduction

Aerial photography has long enjoyed widespread use in glacial geomorphological studies. Satellite remote sensing, however, has not been nearly so common. Limited usage of satellite images can be attributed to its lower spatial resolution and the expense of satellite images and associated computer hardware and software necessary for image processing. This is due in part to remote sensing being oversold as a scientific tool during the early years of the Landsat program (Aber et al., 1993).

However, limitations in application of satellite remote sensing for glacial geomorphological studies, such as high cost and low spatial resolution, are rapidly diminishing. At present, archives of Landsat Multispectral Scanner (MSS) at least two years old and Thematic Mapper (TM) images at least ten years old are again publicly available at reasonable costs for academic research. The upcoming Landsat 7 and EOS ASTER instruments will provide 10-15 m resolution images at low cost in the near future. Numerous commercial satellite are now being built and will provide satellite images with even higher spatial resolution. The increasing power of personal computers and the wide selection of commercial and non-commercial image processing software now available for personal computers allow sophisticated image processing and analysis to be accomplished quite inexpensively.

Satellite images remain unequaled in their ability to provide a regional-scale view of the landscape. They serve both as an excellent basemap for regional studies of alpine glaciation and as a means of placing local field studies within their

regional context. The central Andes of Bolivia, southern Peru, and northern Chile are an excellent area to demonstrate the utility of Landsat TM and MSS images for glacial geomorphological mapping in an alpine environment.

While some detailed field studies have been conducted in the region (e.g. Seltzer, 1992; Clayton and Clapperton, 1995), the inaccessibility of many glaciated areas makes it difficult develop a comprehensive regional picture of late Pleistocene glaciations using traditional field methods. Consequently, regional studies of late Pleistocene glacial extent and snowline elevation (Hastenrath, 1971; Nogami, 1976; Satoh, 1979) are based on limited observations. However, the region's semiarid to arid climate makes it extremely amenable to glacial geomorphological studies using the moderate resolution Landsat TM (28.5 m) and MSS (79 m) sensors. Well preserved moraines and other geomorphological features mark the maximum extent of late Pleistocene glaciers (Seltzer, 1992) and can be easily identified on Landsat images (Fox, 1993).

Satellite images, particularly from the Landsat series of satellites, have been applied to identification of glacial geomorphological features in a variety of settings (e.g. Punkari, 1982; Williams, 1986;Boulton and Clark, 1990; Aber et al., 1993; Clark 1993; Punkari, 1995; Clark, in press). Even using small scale (1:500,000) photographic products, Porter (1985) was able to map the extent of late Pleistocene glaciation in Afghanistan. Use of digital satellite images and image processing techniques allow Landsat images to be effectively employed in mapping glacial geomorphological features at much larger scales of up to 1:50,000.

The aims of the paper are twofold. The first is to describe the image processing techniques involved in the production and utilization of a mosaic of Landsat Thematic Mapper (TM) scenes. The mosaic was used to investigate a wide variety of geomorphological questions, including mapping the extent of alpine glaciation. The radiometric and geometric corrections discussed in this paper are widely used and are described in detail to serve as a guide to preparing images from Landsat and similar sensors (e.g. SPOT) for geomorphological analysis. The paper's second aim is to describe how this regional Landsat TM mosaic is used to estimate and examine important glacier properties including: number, size and volume, as well as to compare the elevation of the late Pleistocene snowline to that at present.

Specifically, a twenty-two scene TM mosaic covering the central Andes from 15°-22° S was used to compile previously-mapped palaeo-glaciers between 18° and 22° S (Fox, 1993) and additional palaeo-glacier mapping covering 15° to 18° S into a single geographic information system (GIS) coverage for analysis. In all, the Landsat mapping revealed that approximately 11,000 palaeo-glaciers occupied the region during the late Pleistocene. Combining the mapping and topographic information complied from topographic maps, the areas and volumes of these former glaciers were estimated. The equilibrium line altitude (ELA) of each individual palaeo-glacier was also determined, yielding the spatial distribution of late Pleistocene ELAs over the region in considerable detail.

This study encompasses the Peruvian-Bolivian Andes between 15° S and 22° S (**Figure 1**). At these latitudes, the Andes are divided into an eastern and a western cordillera, both of which support modern glaciers. The cordilleras are

separated by a large intermontane internally-drained basin of high elevation but low relief known as the Altiplano which is second only to the Tibetan Plateau in height and area.

The ages of the glacial moraines in the region are difficult to constrain because nearly all late Pleistocene glacial dates give only minimum age for deglaciation (Seltzer, 1990). Dates from several sites in the tropical Andes suggest that glaciers reached their maximum extent prior to 20,000 ^{14}C yr BP (Wright, 1983; Mercer, 1984; Seltzer, 1992), but the exact timing is still uncertain. In this study, the glacial chronology of the central Andes is not of primary interest. However, it is assumed that all glacial features identified as late Pleistocene age formed contemporaneously. As the regional glacial chronology continues to improve, this assumption may be found to be incorrect. However, the paucity of glacial dates at present makes it impossible to either confirm or refute this assumption.

The climate of the central Andes is characterized by a lack of significant thermal seasonality and a predominance of the diurnal temperature cycle. Precipitation provides the primary seasonal climate signal in the region. The region has a wet-dry climate associated with the north-south migration of the Intertropical Convergence Zone (ITCZ). A single rainy season extends from October to March. During the remainder of the year, the region receives very little precipitation.

Precipitation, even for the extreme westerly portions of the region, is derived from Atlantic moisture that has been transported from the east across the South

American lowlands. The regional precipitation pattern **(Figure 2)** shows an northeast-southwest decrease in precipitation from the Amazon lowlands (~2000 mm) to the Chilean coast (< 200 mm). Superimposed on this regional decrease are local orographic precipitation extremes occurring on lower eastern Andean slopes. The region's semiarid and prolonged dry season are excellent for remote sensing studies as atmospheric conditions during the dry winter months are commonly clear and cloudless.

Methods

Image Processing

Image processing and geographical information systems (GIS) software was used to map, compile, and analyze the late Pleistocene glacial landforms of the central Andes mapped from Landsat images. Before the images were used for mapping, a radiometrically-corrected and geographically-referenced mosaic was created as a mapping base. While the radiometric and geometric correction of satellite images is an arduous task, it is necessary if satellite images are to be combined with other geographic information in a geographical information system.

Radiometric corrections

In combining Landsat scenes acquired on different dates and under varied atmospheric conditions it is necessary to calibrate the images radiometrically (Lillesand and Kiefer, 1987). Radiometric calibration was performed to convert the radiance measured at the satellite sensor to more physically meaningful units of at-satellite reflectance and to compensate for illumination and atmospheric changes

among the images. These steps were necessary so that image spectra could be compared to laboratory or field spectra (Robinove, 1982) and so computer classification of modern snow cover could be performed across the range of images. From a visual standpoint, radiometric calibration reduces distracting colour variations among the scenes. In the semiarid to arid environments of the central Andes, simple radiometric corrections were found to do an excellent job in allowing multiple images to be merged without unsightly or distracting colour contrasts between the images.

The individual pixels of a Landsat TM and MSS images are quantized into a number of discrete values called digital numbers or DN values. Radiometric correction, discussed in detail by Robinove (1982) and Markham and Barker (1986) and outlined here, involves converting the raw DN values to spectral radiances or reflectances. The first step in radiometrically processing a Landsat TM or MSS image requires converting the raw DN values into units of in-band spectral radiance received at the satellite:

$$L_\lambda = L_{\min \lambda} + \left(\frac{L_{\max \lambda} - L_{\min \lambda}}{DN_{\max}} \right) DN \qquad (1)$$

where L_λ is the spectral radiance in mW cm^{-2} $ster^{-1}$ μm^{-1}, L_{min_λ} is the spectral radiance at DN = 0, L_{max_λ} is the spectral radiance at DN = DN_{max} where DN_{max} is 255 for 8 bit TM data , 127 for 7 bit MSS data, and 63 for 6 bit MSS data. Values for L_{min_λ} and L_{max_λ} used in the TM corrections prior to October 1, 1991 can be found in Markham and Barker (1986). Radiance conversions for scenes produced by

EOSAT after Oct 1, 1991 are detailed in the technical notes at the EOSAT web site: (http://www.spaceimage.com/home/pubs/tech_papers/radiance.html and http://www.spaceimage.com/home/pubs/tech_papers/radcorr.html)

After converting the DN values in each band to a spectral radiance, corrections were made to compensate for varying illumination between scenes acquired at different times of the year and for differences in solar irradiance between bands (Robinove, 1982). This is accomplished by converting the solar radiances (equation 1) to effective at satellite reflectance, or in-band planetary albedo (ρ_p).

$$\rho_p = \frac{\pi L_\lambda d^2}{E_{sun} \cos(\theta_z)} \qquad (2)$$

where ρ_p is the unitless effective at-satellite planetary albedo, L_λ is the spectral radiance, d is the earth sun distance in astronomical units (approximately 1.0), E_{sun} is the mean solar exoatmospheric spectral irradiance (mW cm^{-2} μm^{-1}), and θ_z is the solar zenith angle at the time of image acquisition. The values for E_{sun} for both MSS and TM are given in (Markham and Barker, 1986) or for TM at the EOSAT web site (http://www.spaceimage.com). The solar elevation ($90-\theta_z$) is found in the ancillary files on the digital data tapes. Daily earth-sun distances are published yearly in *The Astronomical Almanac* (e.g. US Naval Observatory, 1996).

It is also necessary to correct satellite images for atmospheric effects as the radiance received at the satellite sensor includes both surface and atmospheric components. The atmosphere affects electromagnetic radiation by scattering,

absorption, and refraction of which scattering processes dominate (Slater et al., 1983). Atmospheric effects are strongly wavelength dependent. Failure to account for relative radiance changes between bands caused by the atmosphere can affect multiband analytical techniques such as band ratioing (Crippen, 1983).

There are two general categories of scattering, Rayleigh and Mie (aerosol). Rayleigh scattering occurs when radiation interacts with air molecules of much smaller diameter than the wavelength and the scattering is inversely proportional to the fourth power of the wavelength (λ^{-4}). The amount of Rayleigh scattering thus depends on the path length through the atmosphere and as such is a function of atmospheric pressure (Fröhlick and Shaw, 1980) or the elevation of the site. Mie scattering occurs when electromagnetic radiation encounters particles with diameters 1/10 to 10 times that of the wavelength. Scattering is roughly proportional to the wavelength to the -0.5 to - 2.5 power (Iqbal, 1983) with a value of -1.3 commonly cited (Angstrom, 1961).

Under typical atmospheric conditions scattering appears to vary between λ^{-2} to $\lambda^{-0.7}$ (Slater et al., 1983; Chavez, 1989). However, scattering in the high dry environments of the central Andes can be reasonably approximated by a simple Rayleigh scattering model. This has also been found true of other arid environments (Chavez, 1988).

Various methods of haze correction are available to remedy these atmospheric effects. Because most geomorphological applications employ previously collected images, atmospheric conditions at the time of image acquisition are

seldom known. Fortunately, this is not a severe problem as most geomorphological studies are primarily interpretive in nature and do not require high radiometric precision. A simple haze correction technique known as blackbody subtraction which requires only image information is usually adequate.

Blackbody subtraction assumes that within each scene there is a high probability that at least some resolution elements or pixels will have no reflectance because they are deeply shadowed. In the absence of atmospheric effects these pixels should have a DN value of 0. The actual DN values in each band for these pixels therefore represents the effect of the atmosphere on the image (Chavez, 1988). In the simplest blackbody correction this DN value for each band is subtracted from all pixels in the image.

One problem with this approach is that the selected correction values may not conform to the realistic relative atmospheric scattering models described above. This problem is avoided by using the improved dark-object subtraction method of Chavez (1988). In this method a DN value is selected in one band and a relative scattering model (usually ranging from λ^{-4} for clear conditions to $\lambda^{-0.5}$ for very hazy conditions) is used to calculate the offset in the remainder of the bands. As the shortest wavelengths (TM band 1 and MSS band 4) usually require the largest corrections, a correction is selected from the image for these bands and the relative scattering model is used to predict the corrections in the remainder of the bands. In the absence of changing vegetation, snow, or cloud cover, these radiometric corrections remove most distracting colour contrasts among scenes and allow

creation of very uniform image mosaics in semiarid to arid environments such as the central Andes.

A colour composite suitable for visual interpretation of geomorphic and geologic features was created by displaying Landsat TM bands 5 (1.55-1.75 μm), 4 (0.76-0.90 μm) and 2 (0.52-0.60 μm) as red, green, and blue respectively. This produced a pseudocolor image with good colour contrast between surface materials but whose colors were similar enough to those in the visible wavelengths to be easily interpretable by individuals with little or no remote sensing expertise. Finally, histogram stretching was employed to enhance the contrast in each of the displayed bands. After the above radiometric corrections had been applied, an identical stretch was applied to each scene in the mosaic and small adjustments were made only to improve the colour matching between scenes affected by thin cirrus clouds.

Geometric Rectification

Combining multiple Landsat images into a single mosaic requires that each individual scene be geometrically rectified into a common map projection. This study employed a Transverse Mercator projection designed to minimize geometric distortions within the central Andes. Each image was transformed into the projection using ground control points (GCPs) which are locations whose geographic position is known and that can be located precisely within the image. Good GCP candidates are cultural features such as road intersections. However, in underdeveloped agrarian landscapes such as the central Andes, cultural features

are scarce and hard to identify. Therefore, natural features such as river junctions were commonly employed as GCPs. Coefficients for two coordinate transformation equations that relate the geographic coordinates to the uncorrected image coordinates were then determined by least-squares regression (Lillesand and Kiefer, 1987). In the absence of independent tests of spatial accuracy, horizontal accuracy is estimated to be on the order of 2-2.5 pixels (approximately 60-75 m). This estimate is based on the root mean square (RMS) errors for the coordinate transformations. The final radiometrically corrected and geometrically rectified Landsat TM mosaic of the central Andes is shown in **Fig. 3** and the scenes comprising the mosaic are listed in **Table 1**.

Glacial geomorphological mapping

Using photo-interpretation, the corrected Landsat Thematic Mapper images were used to map the area encompassed by each palaeo-glacier. The lower limits of each palaeo-glacier were primarily identified by lateral and terminal moraines. Lateral moraines or glacial trimlines defined the middle reaches of the palaeo-glacier and in the upper reaches the extent of each palaeo-glacier was estimated by projecting the lateral moraines or trimlines to the glacier headwall. Approximately 11,000 palaeo-glaciers were mapped in this manner. An ARC/INFO export file containing the mapped palaeo-glaciers and their calculated attributes (see **Appendix I**) is available.

In much of this semiarid region, glacial geomorphological features are well preserved and easily discernible on both TM and MSS images. The higher spatial

resolution and increased spectral content of TM, however, make it superior to MSS for identification of alpine glacier features as can be clearly seen in **Fig. 4**. Over much of the semi-arid portions of the central Andes, lateral moraines can be identified as sharp-crested ridges as is shown in Fig. 4B. Here several lateral moraines are visible both in the aerial photographs and in the Landsat TM image. These narrow moraines are identified by the contrast between a well-illuminated slope facing the sun and the shaded slope on the opposite side of the crest. In many instances, Landsat's lower spatial resolution aids in identification of the large late Pleistocene moraines. Often smaller and less prominent features are not resolved at the 28.5 meter resolution which makes the larger moraines easier to distinguish. The terminal position of the glacier is located by following the lateral moraines to their lowest elevation or to where a terminal moraine is visible. In some areas, several late Pleistocene glacial advances terminated at nearly the same elevation. As the terminal moraines of the earlier glaciations may be more pronounced than those associated with the last glaciation, our mapped glacial extent may be slightly overestimated because the terminal moraines associated with the last advance could not be properly identified.

Another example of identification of moraines on the Altiplano plateau is shown in **Fig. 5**. This area, which lies just to the north-east of La Paz, Bolivia, has been the site of geomorphic field mapping (Argollo, 1980) and provides an informative comparison between our TM-based mapping and field mapping. As can be seen by comparing the Landsat-based mapping (**Figure 5B**) with both aerial photographs (**Figure 5A**) and a portion of the geomorphic map of the region

(Argollo 1980), the Landsat TM based interpretation captures the general pattern of Late Pleistocene glacial extent in the region. The moraine corresponding to the last of the late Pleistocene advances is correctly identified, as are some of the older advances. However, some small features identified as moraines on the TM were mapped in the field by Argollo (1980) as tertiary deposits. In addition some of the earlier glacial advances that extended just past the extent of the last glacial advance were incorrectly identified on the Landsat TM image. As can be seen in aerial photography the topography in this region is quite hummocky which makes discrimination of low relief moraines difficult. However, it should be noted that the areas enclosed by these older and more extensive glaciers were not used in subsequent analysis. Much of the uncertainty in the Landsat analysis stems from the close proximity of moraines of varying ages, all of which have been quite well preserved in this semi-arid climate.

Identification of glacial features in the more humid and vegetated eastern slopes of the eastern cordilleras in Bolivia and in portions of southwestern Peru was more difficult as both areas have extremely high relief. Although modern glaciers are confined to the peaks, late Pleistocene glaciers descended in narrow valleys to much lower elevations. In portions of the eastern cordillera of Bolivia, SPOT panchromatic (10 m) images and aerial photography were used as a check on the TM mapping. Many of the glacial features resolved in the SPOT images and aerial photographs could also be identified in the TM although they were less well defined (**Figure 6)**. The glacial extents visible on these higher resolution images closely

matched those mapped using TM images, lending confidence to our TM-based interpretations.

In these areas, the extent of late Pleistocene glaciation can be mapped by using the regional overview provided by Landsat to interpret individual landforms based on the larger spatial context visible in the Landsat mosaic. An example of identificaton of glacial extent in the eastern cordillera of Bolivia is shown in **Fig. 6**. Here, there is a transition from a U-shaped valley with glacially-scoured bedrock to a much narrower V-shaped valley with less evidence of glacial erosion. Upstream of this transition, it is possible to identify large lateral moraines as crested ridges that are separated from the main valley walls in both the aerial photographs and the Landsat images. Less prominent moraines can often be identified by the shadow that occurs between a lateral moraine and the adjacent valley wall.

The largest problem in the eastern cordillera is identification of the terminal moraine, which may or may not be present. Debris flows, landslide deposits, and river terraces that occur along the valley walls and floor may be mistakenly identified as moraines. In the absence of a clear terminal moraine, the lowest visible evidence of glacial advance must be used to mark the terminal position of the moraine. This is often the shift from a U- to V-shaped valley cross section. However, while the glacial extents in some valleys have undoubtedly been misidentified, Landsat images do reveal, in a manner unobtainable from aerial photographs, the pervasive and identifiable transition from a glacial landscape into a fluvial one throughout the eastern cordillera of Bolivia.

The altitude of the equilibrium line of each palaeo-glacier was estimated using a Toe-to-Headwall Altitude Ratio or THAR (Meierding, 1982) of 0.45. The minimum (toe) and maximum (headwall) elevations used with the THAR to estimate the ELA of each palaeo-glacier were determined by overlaying the mapped glacial extents on the best available topographic maps (1:50,000, 1:100,000, or 1:250,000 topographic maps produced by the Instituto Geografia Militar in La Paz, Bolivia or Lima, Peru). The minimum and maximum elevations within the mapped palaeo-glacier were then recorded.

Modern snow cover classification

In addition to use as a geomorphological mapping base, Landsat TM was used to determine the area of the central Andes covered by modern glaciers and snow cover. These areas were determined using a snow cover classification algorithm developed by Dozier (1989). The radiometric calibration discussed previously allowed a uniform classification criterion to determine if a pixel contained snow or glacial ice. The classification criteria are as follows: reflectance in TM band 1 (0.45-0.52 μm) greater than 15%; reflectance in TM band 5 (1.55-1.75 μm) less than 15%; and the normalized difference ratio between TM band 2 (0.52-0.60 μm) and TM band 5, [(TM2-TM5)/(TM2+TM5)], greater than 0.50. The areas classified as snow and glaciers are shown in **Fig. 7**. As most of the images were collected during the dry winter months, the snow cover shown in the TM mosaic should be near its annual minimum. The modern snowline, which is used as a rough proxy for the elevation of the ELA, was estimated by determining the lower

elevational limit of the classified snow cover. Snowline elevations were recorded every 1-2 km along the lower limit of snow cover to capture the local variability in snowline altitudes (Fox and Bloom, 1994). Modern snowline could not be calculated from the region's glacier inventories because complete spatial coverage was not available.

Results and Discussion

Combining the areas and elevations of the palaeo-glaciers determined from the mapping with similar information about modern glaciers both from the Landsat snowcover classification and glacier inventories enabled a regional comparison between the two states. The properties of primary interest here are the fundamental measurements of area, number, and volume. Of secondary interest is the magnitude and pattern of the elevational change in glaciers between the present and Late Pleistocene.

Glacier area and number

Two of the most easily measured and fundamental properties of a region's glaciers are their area and number. At their late Pleistocene maximum (**Figure 8**), glaciers in the central Andes between 15° and 22° S latitude occupied approximately 29,800 km^2. Based on analysis of the TM-based snow cover classification, snow and glaciers currently occupy approximately 1305 km^2 in the central Andes. As this total includes both snow and glaciers, it is an overestimation of the present glaciated area. Estimates of modern glacierized areas based on glacial inventories in Bolivia (Jordan, 1991), Peru (Hidrandina, 1988), and Chile

(Oyarzun, 1987) indicate that approximately 684 km^2 of the central Andes are glaciated (**Table 2**). Because glacier inventories were not available for two glacierized areas in southwestern Peru, this sum underestimates the total glacierized area. Thus, these two estimates (684 km^2 and 1305 km^2) bracket the area of the central Andes covered by modern glaciers. This area is only a small fraction (2-4%) of the maximum late Pleistocene glaciated area.

At present, approximately 1500 glaciers exist in the central Andes from 15° to 22° S with the majority (1174+) found in the eastern cordilleras of Bolivia (Jordan, 1991). In the Chilean Andes between 18° and 22° S, Oyarzun (1987) inventoried 22 glaciers and the western cordilleras of Bolivia contain a few additional glaciers (Jordan, 1991). The number of glaciers existing in Peru south of 15° is unknown because of an incomplete glacier inventory in Peru. Excluding unsurveyed areas, Peruvian glaciers within the study region number approximately 340 (Hidrandina, 1988).

In contrast, at their late Pleistocene glacial maximum, approximately 11,000 glaciers existed in the central Andes. While there is uncertainty in this estimate arising from subjective decisions made in the mapping process concerning whether individual ice masses should be split or joined, the number of late Pleistocene glaciers was nearly an order of magnitude greater than those presently existing in the central Andes. These glaciers were considerably larger as well. The largest modern glacier within the entire Peruvian and Bolivian Andes is 16.5 km^2. In contrast. the largest mapped Late Pleistocene glacier covered an area of 264 km^2

(**Table 3**). Both the mean and median sizes of the late Pleistocene glaciers were larger as well, indicating an overall increase in glacier size.

Area-Number scaling

A current topic of research in quantitative geomorphology is the study of the scale-invariant nature of many elements of the landscape. Scale-invariant phenomena are characterized by a power-law, fractal distribution (Turcotte, 1992). However, examination of the cumulative distribution of glacier area versus number for different regions of the world reveals that glacier size deviates markedly from a power-law distribution. Instead, the cumulative size distribution of glaciers appears to approximate the product of a power-law and an exponential. However, the physical basis for this distribution is unknown (Meier and Bahr, 1996).

In a log/log plot of area versus cumulative number, this fractal-exponential relationship is characterized by a convex-up curve rather than a straight-line indicative of scale-invariance. The area-cumulative number relationship of both modern and palaeo-glaciers in the central Andes is similar to that of glaciers from other areas of the world (**Figure 9)**.

The area-number distribution for modern glaciers was calculated from the glacier inventories of Peru and Bolivia (World Glacier Monitoring Service, unpublished data). The curves of modern Peruvian and Bolivian glaciers parallel each other (**Figure 9**), indicating that while the mean sizes differ (as is shown in **Table 3**), their relative size distributions are similar. The relationship between glacier size and number for late Pleistocene glaciers in the central Andes also

follows the fractal-exponential relationship. However, the ratio of large glaciers to small ones was slightly greater during late Pleistocene times than at present. This is what would be expected if smaller glaciers coalesced into larger glacier systems during the late Pleistocene. However, it could also be an artifact resulting from lumping small individual glaciers into larger ice bodies during the mapping process. Despite the differences in size distribution between modern and late Pleistocene glaciers, their overall similarity provides some measure of confidence that Landsat TM-based glacier mapping is an accurate representation of late Pleistocene glaciers in the central Andes.

Ice volume of late Pleistocene and modern glaciers

In addition to determining the size of late Pleistocene glaciers in the central Andes, it is important to estimate their equivalent ice volume. In particular, the effect of glacial meltwater on the paleolakes of the Altiplano has received considerable attention (e.g. Kessler, 1983; Hastenrath and Kutzbach, 1985; Clayton and Clapperton, 1995; Blodgett et al., 1996). Determining the volume of glacial ice requires a knowledge of how glacier volume scales as a function of area.

A statistical relationship between the area of late Pleistocene glaciers in the central Andes and their volume has been previously developed by Fox (1993). The relationship was established by reconstructing the ice surface of sixty-nine glaciers in southern Bolivia following the method developed by Porter (1975) and subtracting the elevation of the underlying topography in a GIS. For the entire

central Andes, ice volume estimated using this relationship is 4347 km^3. However, no physical basis exists for this empirically-derived relationship (**Figure 10**).

Recent empirical (Meier and Bahr, 1996) and theoretical (Bahr et al., 1996) studies indicate that for modern temperate glaciers, volume scales as an exponential function of area:

$$V = cA^b \quad (3)$$

where V is volume, A is area, and c and b are scaling factors. The empirically determined exponential scaling factor (b = 1.36) has been found to have a theoretical basis (Bahr et al., 1996). The area-volume relationship of the sixty-nine reconstructed glaciers conforms to this exponential relationship (**Figure 10**). Through least-squares curve fitting, the linear scaling term (c) was estimated to be 0.048. Equation (3) allowed the total ice volume of late Pleistocene glaciers to be more confidently estimated as 3676 km^3. The large difference (15%) in ice volume estimates is caused by the greater volumes estimated for of the largest and smallest glaciers by the Fox (1993) equation.

Using equation (3) , the coefficients developed for the palaeo-glaciers and Bolivian glacier inventory data (World Glacier Monitoring Service, unpublished data), the volume of modern Bolivian glaciers in the central Andes south of 15^o S were determined. The total volume of Bolivian glaciers is estimated to be 17.5 km^3. Given that the total area of these glaciers is approximately one-half of the total glacierized area, the total volume of the region's glaciers is perhaps 2-3 times this or 35 to 53 km^3. Despite the obvious uncertainties in this estimate, it is nevertheless

only a minute fraction (1.0-1.2%) of the volume of the region's late Pleistocene glaciers.

Regional ELA pattern and depressions

The regional view of the central Andes provided by Landsat TM images has enabled reconstruction of the elevation of the late Pleistocene ELA.. By comparing the regional ELA patterns of late Pleistocene glaciers with those at present, the regional pattern of ELA lowering (snowline depression) was calculated. The amount of ELA lowering varies considerably across the central Andes and this fact has important consequences for paleoclimatic interpretations based on ELA depressions.

Both modern (**Figure 11**) and late Pleistocene (**Figure 12**) ELAs show a rise northeast to southwest across the central Andes. Modern ELA rises steeply from ~4500 m to over 5000 meters across the eastern cordillera of Bolivia then rises more gently across the Altiplano to extremely high elevations (>5800 m) along the Bolivia-Chile border. This rise in modern ELA is a direct consequence of decreasing precipitation across the region (Kuhn, 1980).

Late Pleistocene ELA also rose steeply across the eastern cordillera then gently rose southwest across the plateau to >4800 m in the western cordillera. In southwestern Peru and northern Chile, there was a slight drop in the elevations of the late Pleistocene equilibrium line along the western slopes of the western cordillera. Like their modern counterparts, in areas where the precipitation gradient is steep (**Figure 2**), such as along the eastern Cordillera in Bolivia, the

late Pleistocene ELA rose quickly and where the east-west precipitation gradient is gentler, the rise in ELA was more gradual. This indicates that at the time of the local glacial maximum, precipitation in the central Andes had a predominately easterly source as today as concluded by Fox (1993).

The equilibrium line of late Pleistocene glaciers was 500-1200 m lower than today (**Figure 13**). The lowering was greatest along the eastern cordillera of Peru and Bolivia where the ELA was consistently 1000-1200 m lower. This uniform depression is the best proxy for the late Pleistocene temperature change and is consistent with a 5-9°C cooling (Klein et al., 1995; Klein, 1997).

A 1000 m or more lowering of the equilibrium line also occurred in the western cordillera. Presently the glaciers in this region are confined to extremely high altitudes and are thought to be much more sensitive to precipitation changes than to temperature changes (Kuhn, 1980; Kaser, 1995). The high sensitivity to precipitation changes makes a precipitation increase the most likely explanation for the large ELA lowering observed in this arid region as has been previously hypothesized (Hastenrath, 1971; Wright, 1983). Because precipitation is thought to be more important than temperature in controlling the altitude at which modern glaciers are found in the arid western cordillera, the idea that extensive late Pleistocene glacier expansion occurred under much drier conditions as hypothesized by Fox and Bloom (1994) and Satoh (1979) appears unreasonable.

The late Pleistocene ELA depression in the central Andes was considerably more complicated than the uniform 1000 m often assumed for the tropics (Rind and Peteet, 1985; Broecker and Denton, 1989). For example, ELA depression over much

of the Altiplano was much less than 1000 m. Areas of southeast Peru and Bolivia experienced only 500 to 800 meters of ELA lowering. These areas of small ELA lowering correspond to areas of high elevation but low relief (**Figure 1**) and suggest that high plateaus limit the elevation to which glaciers descended during the late Pleistocene. The coincidence of multiple phases of glaciation reaching nearly the same elevation along the western slope of the Cordillera Real, Bolivia (Gouze et al., 1986; Seltzer, 1992) is another indication that the Altiplano and other regions of high elevation but low relief cause a non-climatic threshold to limit glacier expansion as noted by Clapperton (1981)

Conclusions

The regional view provided by Landsat Thematic Mapper images provides an effective tool for identification and mapping of late Pleistocene glacial features on a regional scale in the semiarid central Andes. Simple radiometric and geometric corrections are all that are required to integrate multiple TM scenes into a single seamless mosaic that can be used for regional scale geomorphological mapping.

A Landsat Thematic Mapper image mosaic of the central Andes was used to map the extent of late Pleistocene moraines in the central Andes and allowed the magnitude and pattern of ELA (snowline) depression to be determined on a regional scale. Modern and late Pleistocene ELAs exhibit a similar northeast to southwest rise in elevation that is a response to decreasing precipitation across the region. The magnitude of ELA depression on a regional scale was found to vary considerably from the uniform 1000 m lowering often assumed for tropical latitudes.

The lowering was greatest along the eastern cordillera of Peru and Bolivia where the ELA was consistently 1000-1200 m lower. This depression is the best proxy for the late Pleistocene temperature change and has been found to be consistent with a 5-9°C cooling.

The remote sensing techniques used here are equally applicable to mapping late Pleistocene glacier features in other remote semiarid environments such as the Tibetan Plateau and the Atlas mountains of north Africa. As the cost of using satellite images decreases and the spatial resolution increases, satellite images can only become more important in geomorphological studies.

Acknowledgments

This work is supported by the NASA mission to Planet Earth/Earth Observing System grant NAGW-2638 as well as support from the DOE Graduate Fellowship for Global Change Program. My thanks go to the present and former members of the Cornell Andes project, especially Eric Fielding and Timothy Gubbels, who helped make the Cornell University Landsat archive accessible to all. I also am indebted to James Aber for discussions on the subject. Glacier inventory data for Peru and Bolivia were kindly provided by W. Haeberli and M. Hoelzle of the World Glacier Monitoring Service.

References

Aber, J.S., Spellman, E.E. and Webster, M.P. 1993 Landsat Remote Sensing of Glacial Terrain. In: J.S. Aber (ed.), Glaciotectonics and Mapping Glacial Deposits: Proceedings of the INQUA Commission on Formation and Properties of Glacial Deposits, Canadian Plains Research Center, University of Regina, pp. 215-225.

Angstrom, A. 1961 Techniques of determining the turbidity of the atmosphere. Tellus, 13, 214-231.

Argollo, B.J. 1980 Los Pie de Montes del al Cordillera Real entre los Valles de la Paz y de Tuni, Estudio Geológico, Evolución Plio-Cuaternaria. Teis De Grado, Universidad Mayor de San Andrews, La Paz, Bolivia.

Bahr, D.B., Meier, M.F. and Peckham, S.D. 1996 The physical basis for glacier volume-area scaling and implications for mass balance profiles. In: S.C. Colbeck (ed.), Glaciers, Ice Sheets and Volcanoes: A Tribute to Mark F. Meier. CRREL, Hanover, NH, pp. 11.

Blodgett, T., Lenters, J.D. and Isacks, B.L. 1996 Constraints on the origin of paleolake expansions in the central Andes: results from GIS and evaporation model analysis. Earth Interactions, E1, [availble at http://EarthInteractions.org].

Boulton, G.S. and Clark, S.D. 1990 A highly mobile Laurentide ice sheet revealed by satellite images of glacial lineations. Nature, 346, 813-817.

Broecker, W.S. and Denton, G.H. 1989 The role of ocean-atmosphere reorganizations in glacial cycles. Geochimica et Cosmochimica Acta, 53, 2465-2501.

Chavez, P.S. Jr.1988 An improved dark-object subtraction technique for atmospheric scattering correction of multispectral data. Remote Sensing of Environment, 24, 459-479.

Chavez, P.S. Jr. 1989 Radiometric calibration of Landsat Thematic Mapper multispectral images. Photogrammetric Engineering and Remote Sensing, 55, 1285-1294.

Clapperton, C.M. 1981. Quaternary glaciations in the Cordillera Blanca, Peru and the Cordillera Real, Bolivia, Revista CIAF (Bogota) 6, 93-111.

Clark, C.D. in press Reconstructing the evolutionary dynamics of former ice sheets using multi-temporal evidence, remote sensing and GIS. Quaternary Science Reviews.

Clark, C.D. 1993 Mega-scale glacial lineations and cross-cutting ice-flow landforms. Earth Surface Processes and Landforms, 18, 1-29.**Clayton, J.D. and**

Clapperton, C.M. 1995 The last glacial cycle and palaeolake synchrony in the southern Bolivian Altiplano: Cerro Azanaques case study. Bull. Inst. fr. études andines, 24, 563-571.

Crippen, R.E. 1983 The dangers of underestimating the importance of data adjustments in band ratioing. International Journal of Remote Sensing, 9, 767-776.

Defense Mapping Agency 1989 Digital Chart of the World Database (MIL-D-89009). U.S. Government Printing Office, Washington, D.C.

Dozier, J. 1989 Spectral signature of alpine snow cover from the Landsat Thematic Mapper. Remote Sensing of Environment, 28, 9-22.

Fox, A.N. 1993 Snowline altitude and climate in the Central Andes (5-28°S) at present and during the Late Pleistocene Glacial Maximum. Ph.D. Thesis, Cornell University.

Fox, A.N. and Bloom, A.L. 1994 Snowline altitude and climate in the Peruvian Andes (5-17° S) at present and during the Latest Pleistocene Glacial Maximum. Journal of Geography (Japan), 103, 867-885.

Fröhlich, C. and Shaw, G.E. 1980 New determination of Rayleigh scattering in the terrestrial atmosphere. Applied Optics, 19, 1773-1775.

Gouze, P., Argollo, J., Saliege, J.-F. and Servant, M. 1986 Interprétation paléoclimatique des oscillations des glaciers au cours des 20 derniers millénaires dans les régions tropicals; exemple des Andes boliviennes. Academie de Sciences, 303, 219-223.

Hastenrath, S. 1971 On the Pleistocene snow-line depression in the arid regions of the South American Andes. Journal of Glaciology, 10, 225-267.

Hastenrath, S. and Kutzbach, J.E. 1985 Late Pleistocene climate and water budget of the South American Altiplano. Quaternary Research, 24, 249-256.

Hidrandina 1988 Glacier Inventory of Peru, Consejo Nacional de Ciencia y Tecnologia (CONCYTEC), Huaraz.

Hoffman, J.A.J. 1975 Climatic Atlas of South America. WMO, UNESCO, Geneva.

Iqbal, M. 1983 An Introduction to Solar Radiation. Academic Press, Toronto.

Isacks, B.L. 1988 Uplift of the Central Andean Plateau and bending of the Bolivian Anticline. Journal of Geophysical Research, 93, 3211-3231.

Jordan, E. 1991 Die Gletscher der bolivianischen Andean. Franz Steiner Verlag Stuttgart, Eurasburg, Germany.

Kaser, G. 1995 Some notes on the behavior of tropical glaciers. Bull. Inst. fr. études andines, 24, 671-681.

Kessler, A. 1983 The paleohydrology of the late Pleistocene lake Tauca on the Bolivian Altiplano and recent climatic fluctuations., SASQUA International Symposium, Swaziland, pp. 115-122.

Klein, A.G. 1997 Modern and late Pleistocene glacial studies in the central Andes of Peru and Bolivia: application of satellite remote sensing and digital terrain analysis. Ph.D. Thesis, Cornell University, Ithaca, NY, 191 pp.

Klein, A.G., Isacks, B.L. and Bloom, A.L. 1995 Modern and last glacial maximum snowline in Peru and Bolivia: Implications for regional climatic change. Bull. Inst. fr. études andines, 24, 607-617.

Kuhn, M.V. 1980 Vergletscherung, Nullgradgrenze und Niederschlag in den Anden, Jahrbuch des Sonnblickvereins, 1978-1979. Springer Verlag, Wien, pp. 1-13.

Lillesand, T.M. and Kiefer, R.W. 1987 Remote Sensing and Image Interpretation. John Wiley & Sons, New York.

Markham, B.L. and Barker, J.L. 1986 Landsat MSS and TM post-calibration dynamic ranges, exoatmospheric reflectances and at satellite temperatures. EOSAT Technical Notes, 1, 3-8.

Meier, M.F. and Bahr, D.B. 1996 Counting glaciers: use of scaling methods to estimate the number and size distribution of the glaciers of the world. In: S.C. Colbeck (ed.), Glaciers, Ice Sheets and Volcanoes: A Tribute to Mark F. Meier. CRREL, Hanover, NH, pp. 89-94.

Meierding, T.C. 1982 Late Pleistocene glacial equilibrium-line altitudes in the Colorado Front Range: a comparison of methods. Quaternary Research, 18, 289-310.

Mercer, J.H. 1984 Late Cainozoic glacial variations in South America south of the equator. In: J.C. Vogel (ed.), Late Cainozoic Palaeoclimates of the Southern Hemisphere. A.A. Balkema, Rotterdam, pp. 45-58.

Nogami, M. 1976 Altitude of the modern snowline and Pleistocene snowline in the Andes. Tokyo Metropolitan University Geographical Reports, 11, 71-86.

Oyarzun, C.G. 1987 Inventario do Glaciares de los Andes Chilenos desde los 18° a los 32° de Latitud Sur. Revista de Geografia Norte Grande, 14, 35-48.

Porter, S.C. 1985 Extent of Late Pleistocene glaciers in Afghanistan based on interpretation of Landsat imagery. In: D.P. Argrawal (ed.), Climate and Geology of Kashmir, the last 4 million years; proceedings of the international workshop on the

Late Cenozoic palaeoclimatic changes in Kashmir and central Asia. Current Trends in Geology, pp. 191-195.

Porter, S.C. 1975 Equilibrium-line altitudes of Late Quaternary glaciers in the Southern Alps, New Zealand. Quaternary Research, 5, 27-47.

Punkari, M. 1995 Glacial flow systems in the zone of confluence between the Scandinavian and Novaya Zemlya ice sheets. Quaternary Science Reviews, 14, 589-603

Punkari, M. 1982 Glacial geomoprhology and dynamics in the eastern parts of the Baltic Shield interpreted using Landsat imagery. Photogrammetric Journal of Finland, 9, 77-93.

Rind, D. and Peteet, D. 1985 Terrestrial conditions at the Last Glacial Maximum and CLIMAP sea surface temperature estimates: are they consistent? Quaternary Research, 24, 1-22.

Robinove, C.J. 1982 Computation with physical values from Landsat digital data. Photogrammetric Engineering and Remote Sensing, 48, 781-784.

Satoh, H. 1979 On the Snow-line Altitude in the Central and Southern Andes of the Modern Age and the Diluvial Epoch. In: S. Horie (ed.), Paleolimnology of Lake Biwa and the Japanese Pleistocene, pp. 387-415.

Seltzer, G.O. 1990 Recent Glacial History and Paleoclimate of the Peruvian-Bolivian Andes. Quaternary Science Reviews, 9, 137-152.

Seltzer, G.O. 1992 Late Quaternary glaciation of the Cordillera Real, Bolivia. Journal of Quaternary Science, 7, 87-98.

Slater, P.N., Doyle, F.J., Fritz, N.L. and Weltch, R. 1983 Photographic systems for remote sensing. In: R.N. Colwell (ed.), Second Edition of Manual of Remote Sensing. American Society of Photogrammetry, pp. 231-291.

Turcotte, D.L. 1992 Fractals and Chaos in Geology and Geophysics. Cambridge University Press, Cambridge.

U.S. Naval Observatory 1996 The Astronomical Almanac. U.S. Government Printing Office, Washington, D.C.

Williams, R.S. Jr. 1986 Glacier inventory of Iceland: Evaluation and use of sources of data. Annals of Glaciology, 8, 184-191.

Wright, H.E. 1983 Late-Pleistocene Glaciation and Climate Around the Junin Plain, Central Peruvian Highlands,. Geografiska Annaler, 65 A, 35-43.

Figure Captions

Figure 1: Colour-coded, shaded-relief topography of the central Andes of Bolivia, Peru, and northern Chile (Isacks, 1988; Defense Mapping Agency, 1989)

Figure 2. Mean annual precipitation of the central Andes of Bolivia, Peru, and northern Chile (Hoffman, 1975). Contours are in millimeters and are colour coded from wettest (purple) to driest (red).

Figure 3: Pseudocolor Landsat Thematic Mapper mosaic of the central Andes of Bolivia, Peru, and northern Chile. Landsat bands 5, 4, and 2 are displayed as red, green and blue respectively. Modern glaciers and snowcover appear in cyan. The red boxes indicate the location of **Figs. 4**, **5** and **6**.

Figure 4: **(A)** Monochromatic (TM band 4 and MSS band 7) example showing an example of moraine identification using Landsat Thematic Mapper (left) and Landsat Multispectral Scanner images (right) for Nevado Sajama, Bolivia. The white outline represents the extent of late Pleistocene glaciers mapped using TM. While the moraine crests are quite sharp in the TM image, the are not nearly as well defined in the lower resolution MSS image (insets). **(B)** A comparison of the appearance of moraines on a Landsat TM image (left) and aerial photograph (right). In both images the sharp crested moraines are clearly visible. In some cases, the larger contrast in tone due to shadowing and blurring of smaller-scale features in the Landsat TM image makes identification of the large late Pleistocene moraines easier than on aerial photographs.

Figure 5: A comparison of **(A)** aerial photography, **(B)** Landsat TM, **(C)** a terrestrial photography and **(D)** a field based geomorphic map published by Argollo (1980) for an area north-east of La Paz, Bolivia. Overall the correspondence between moraines mapped from Landsat TM and those mapped in the field (red Choqueyapu moraines) is quite good. Some of the older moraines, however, have been misidentified on the Landsat image. As can be seen in the terrestrial photograph, these late Pleistocene glaciers were quite large and left behind large lateral and terminal moraines.

Figure 6: A comparison of aerial photography **(A)** and Landsat TM (28.5) images **(B and C,** respectively**)**for an small area in the rugged eastern cordillera of Bolivia. Many features, including moraines, valley form and glacially-scoured bedrock, that are visible in aerial photographs are also recognizable in Landsat images and can be used to map the extent of late Pleistocene glaciation in the area. The mapped glacial extents are shown in **(C)**. Note that the major goal of the study was to identify the minimum and maximum elevations encompassed by each late Pleistocene glacier, not to create minutely detailed representation of each glacier; therefore the glacial extents are somewhat generalized.

Figure 7: Modern snow cover extent (black) in the central Andes calculated from the Landsat Thematic Mapper images shown in **Figure 3**. The large lakes and salars (salt flats) in the region are shown in blue.

Figure 8: Late Pleistocene glacier extent (blue) in the central Andes mapped from Landsat Thematic Mapper images shown in **Figure 3**.

Figure 9: **(A)** a cumulative frequency plot of the size (km^2) of modern (Bolivia-green; Peru-red) and late Pleistocene glaciers (blue) in the central Andes of Peru and Bolivia versus number (N_c). The cumulative frequency plot for the Alps (large blue-gray dots) is also shown. **(B)** identical to **(A)** except each curve has been normalized by the total number of glaciers to accentuate differences in curvature.

Figure 10: Area volume relationship for the sixty-nine reconstructed late Pleistocene glaciers (Fox, 1993). The solid blue curve is the area-volume relationship developed for modern glaciers by (Meier and Bahr, 1996). The dashed red line represents the original empirical relationship determined by Fox. The curvature in the Fox (1993) relationship causes excessive volumes to be estimated for glaciers with areas outside the sampled sizes. Because many glaciers of these sizes do exist, the use of the area-volume relationship developed by Meier and Bahr (1996) is preferable.

Figure 11: Modern snowline elevation in the central Andes based on the classified snow cover shown in **Figure 7**. The contours were created by averaging individual elevation estimates in a 0.25° x 0.25° moving window and hand contouring the resulting values. Contour interval is 100 m.

Figure 12 Late Pleistocene equilibrium line altitudes in the central Andes based on the glaciers shown in **Figure 8**. The contours were calculated by determining the minimum snowline elevation within a moving 0.25° x 0.25° moving window and then contouring. Contour interval is 200 m.

Figure 13: Late Pleistocene ELA depression in the central Andes. The ELA depression was calculated by creating continuous surfaces of modern and late

Pleistocene ELA surfaces based on the contours shown in **Figure 11** and **12**. The depression is a simple difference between the two that has been smoothed with a low pass filter to remove high frequency noise. Contour interval 100 m.

Table 1: Landsat Thematic Mapper Images comprising the central Andes Mosaic

Path	Row	Scene-ID	acquisition date	solar elevevation (degrees)
1	71	51249-14004	8/2/87	38
1	72	50129-14040	7/8/84	35
1	73	51185-14000	5/30/87	35
1	74	50913-13571	8/31/86	41
1	75	51073-13570	2/7/87	48
2	70	50472-14105	6/16/85	37
2	71	50520-14110	8/2/85	39
2	72	50920-14022	9/7/86	45
2	73	50392-14122	3/28/85	46
3	70	50511-14165	7/25/85	39
3	71	50447-14173	5/22/85	39
3	72	50383-14181	3/19/85	48
4	71	50502-14233	7/16/85	37
5	71	50381-14301	3/17/85	49
231	74	50492-13474	7/6/85	32
231	75	50396-13482	4/1/85	43
232	73	50803-13481	5/13/86	37
232	74	50867-13463	7/16/86	32
232	75	50771-13494	4/11/86	41
233	72	50474-13592	6/18/85	35
233	73	50522-13592	8/5/85	38
233	74	50474-14001	6/18/85	32
233	75	50522-14001	8/5/85	35

Table 2: Number and area of modern glaciers found within the central Andes 15°-22° S.

Region	Subregion	Number	Area (km^2)
Central Andes		**1539**	**684.37**
Bolivia[1]		**1174+**	**369.72**
eastern cordillera		*1174*	*356.72*
	Cordillera de Munecas	16	0.68
	Cordillera Real	985	317.16
	Tres Cruces	156	36.65
	Santa Vera Cruz	17	2.23
Western cordillera		*unknown*	*13*
	Nevado Condoriri	*unknown*	2
	Nevado Sajama	*unknown*	4
	Nevaods Payachata	*unknown*	5
	Mevdo Quimsa Chata	*Unknown*	2
Peru[2]		**343**	**228.82**
	Ampato	93	146.73
	Huanzo	115	36.93
	Chila	87	33.89
	La Raya	48	11.27
	Volcanica	Unknown	Unknown
	Barroso	Unknown	Unknown
Chile[3]	18°-22°S	**22**	**85.83**

[1]Jordan (1991), [2]Hidrandina (1988), [3]Oyarzun (1987)

Table 3: Area statistics of modern glaciers and Late Pleistocene palaeo-glaciers in the central Andes (World Glacier Monitoring Service, unpublished data)

	Mean area (km^2)	median area (km^2)	standard deviation (km^2)	minimum area (km^2)	maximum area (km^2)	number
Peru	0.67	0.25	1.24	0.01	16.50	1,679
Bolivia	0.34	0.07	0.82	0.01	10.32	1,501
Palaeo	2.72	0.87	8.01	0.001	264.31	10,941

Appendix I: Palaeo-glacier maps

The mapped late Pleistocene glacier extents are included as an ARC/INFO interchange (export) file. The projection is GEOGRAPHIC, the datum WGS84, and the map units DECIMAL DEGREES. The coverage contains the following attributes for each glacier:

Attribute	Description	Units
AREA	Area of glacier polygon	km^2
PERIMETER	Perimeter of glacier polygon	km
PG_BOL_DDF4#	Internal ARC/INFO number	
PG_BOL_DDF4-ID	Glacier polygon identification number	
X_COORD	Longitude of glacier polygon label	Decimal degrees
Y_COORD	Latitude of glacier polygon label	Decimal degrees
MIN	Minimum Elevation in Glacier Polygon	m
MAX	Maximum Elevation in Glacier Polygon	m
MEAN	(MIN-MAX)/2.0	m
THAR45	Elevation corresponding to a THAR of 0.45: MIN + 0.45(MAX-MIN)	m
LONG	Longitude of glacier polygon label	Decimal degrees
LAT	Latitude of glacier polygon label	Decimal degrees

GLACAREA	Glacier Polygon Area	km^2
GLACVOL	Glacier Volume calculated as $0.048GLACAREA^{1.36}$	km^3
MAPSCALE	Scale of the Map used to determine MIN and MAX elevations	

Appendix II: Pertinent World Wide Web Sites

The United States Geological Survey's EROS Data Center, Sioux Falls, South Dakota, USA, maintains an online, interactive database (webglis). This database contains product descriptions, pricing, ordering information, and a geographic search and browse capability for Landsat MSS and TM images as well as host of other data: http://edcwww.cr.usgs.gov/webglis

The Landsat home page contains information about past, current and future Landsat satellites: http://geo.arc.nasa.gov/sge/landsat/landsat.html

The ASTER instrument which is scheduled to fly on the first EOS-AM platform also has a home page: http://asterweb.jpl.nasa.gov

The Department of Geological Sciences at Cornell University maintains an index and viewable "quicklooks" of its collection of Landsat TM images of the Andes: http//www.geo.cornell.edu/geology/cap/TMscenes.html

A web site focusing on Quaternary Research in South America is maintained by Dr. Geoffrey Seltzer at Syracuse University:
http://web.syr.edu/~goseltze/sac.html

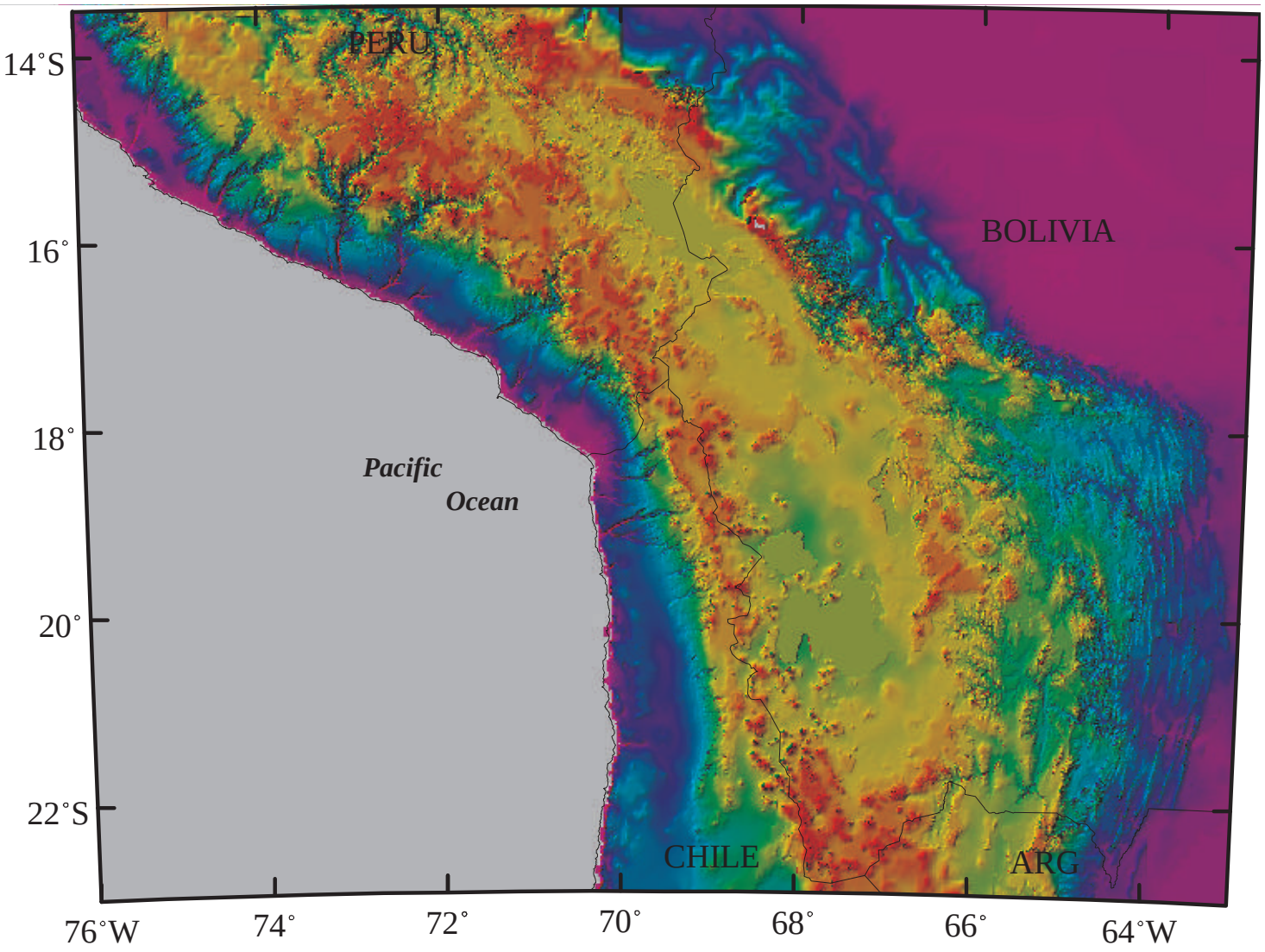
PERU
BOLIVIA
Pacific
Ocean
CHILE
ARG
14˚S
16˚
18˚
20˚
22˚S
76˚W
74˚
72˚
70˚
68˚
66˚
64˚W

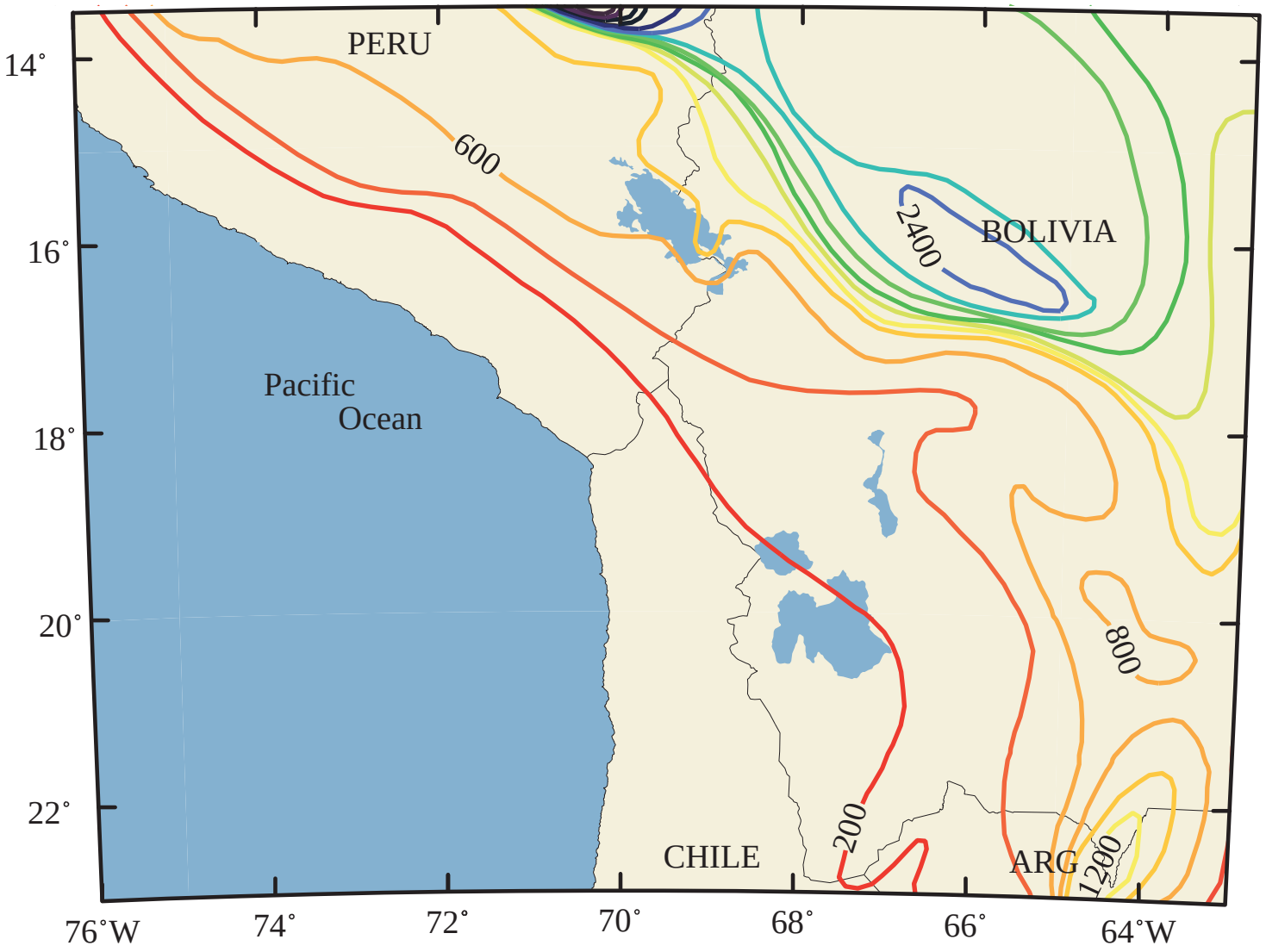
PERU
BOLIVIA
Pacific
Ocean
CHILE
ARG
600
2400
800
200
1200
14˚
16˚
18˚
20˚
22˚
76˚W
74˚
72˚
70˚
68˚
66˚
64˚W

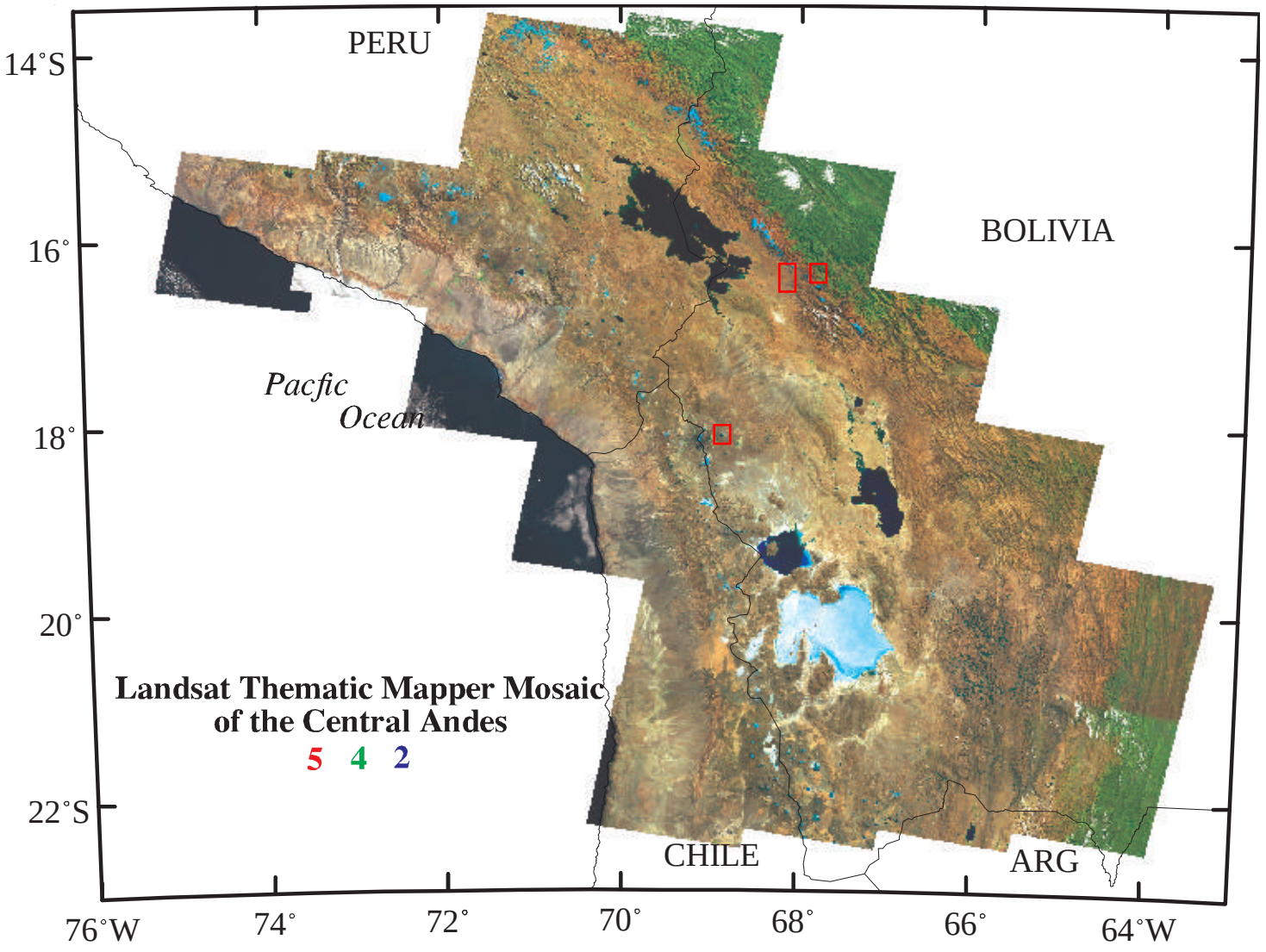
PERU
BOLIVIA
Pacfic
Ocean
CHILE
ARG
14˚S
16˚
18˚
20˚
22˚S
76˚W
74˚
72˚
70˚
68˚
66˚
64˚W
Landsat Thematic Mapper Mosaic
of the Central Andes
5 4 2

A

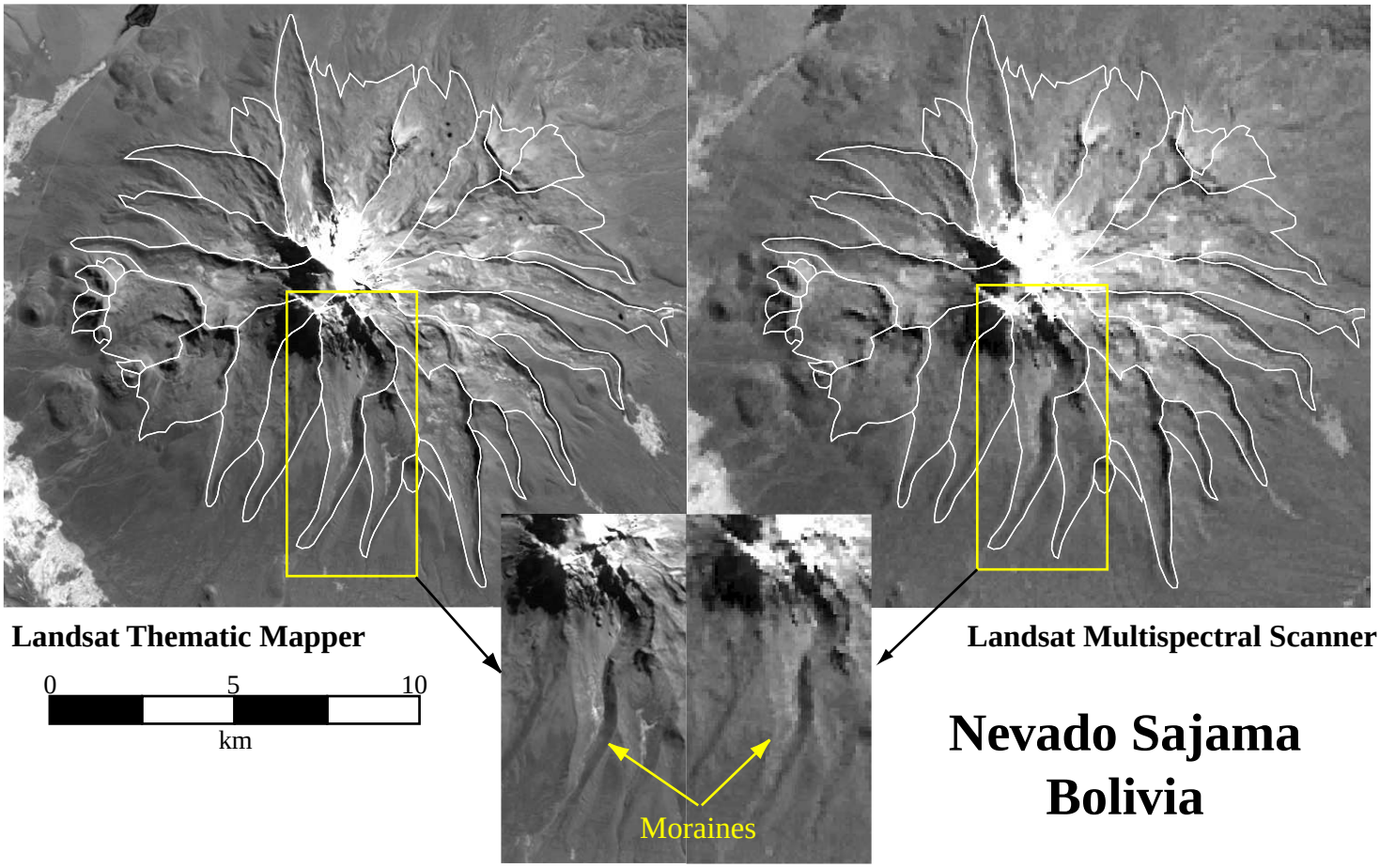

B

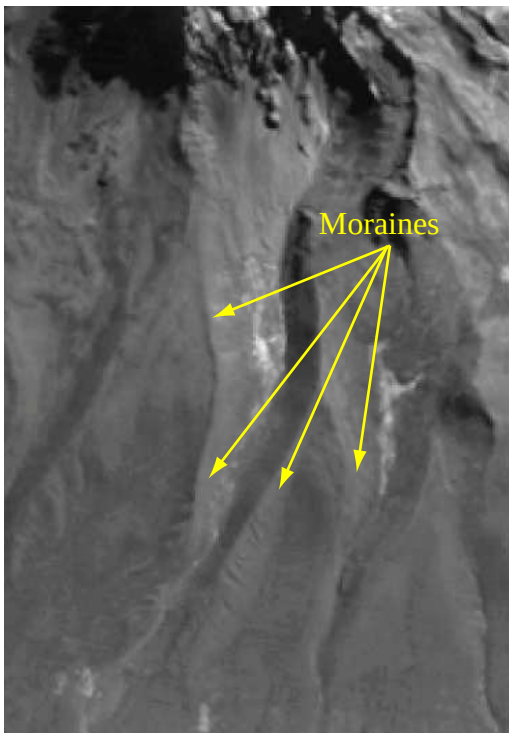

Landsat Thematic Mapper
(path 001 row 73)

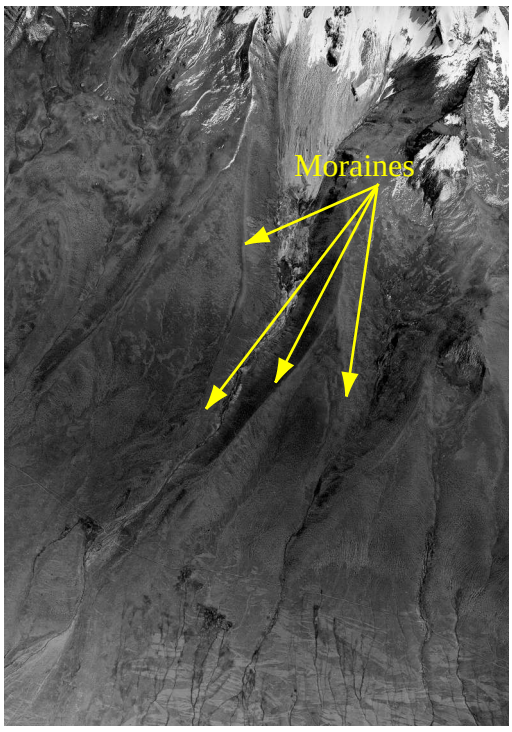

Aerial Photograph
(31-Jul-63)

A

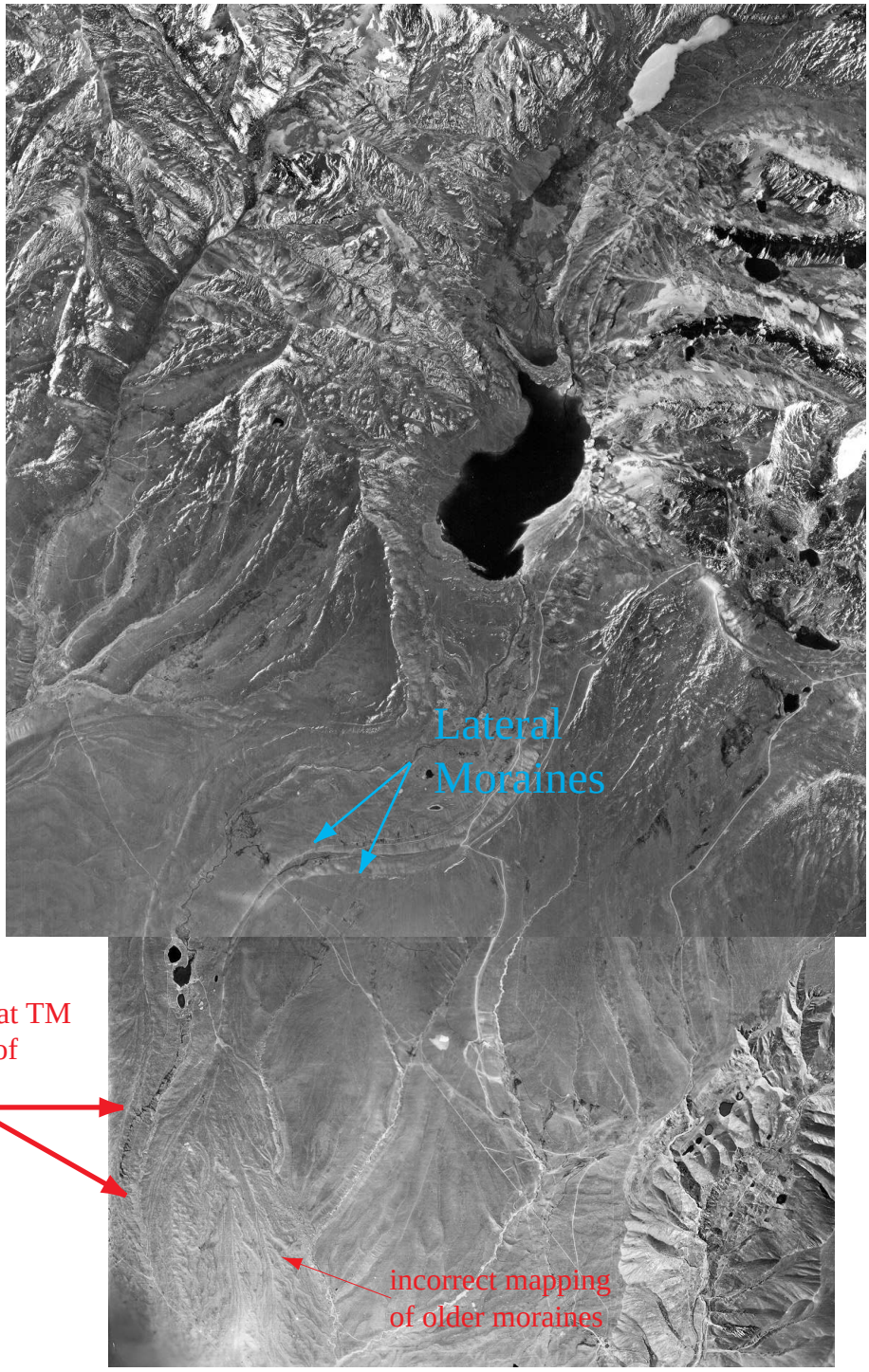
Lateral
Moraines
Ambiguity in Landsat TM
as to exact location of
terminal moraine
incorrect mapping
of older moraines

A

B


Terrestrial Photograph
Location and direction
Lateral
Moraines
older ice extents slightly
inaccurately mapped
Ambiguity in Landsat TM
as to exact location of
terminal moraine
incorrect mapping
of older moraines

C

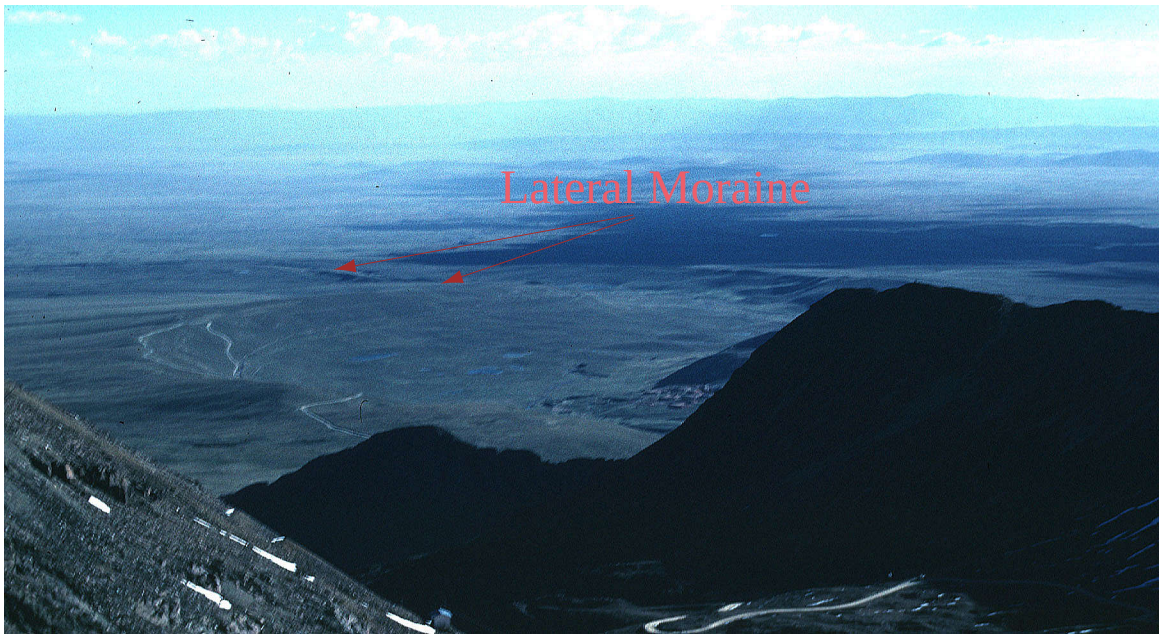

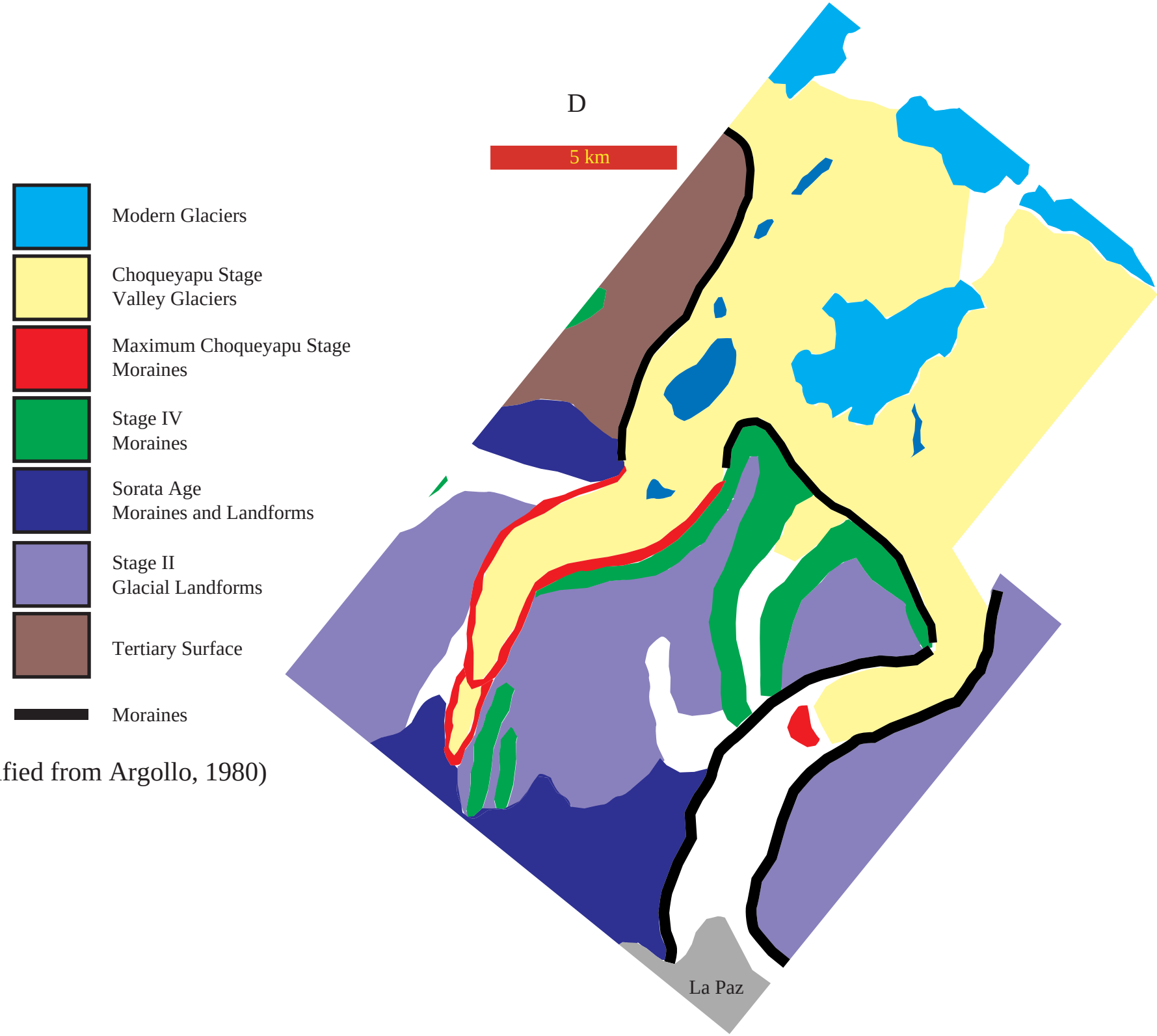

(Modified from Argollo, 1980)

Aerial Photograph
(20-May-56)

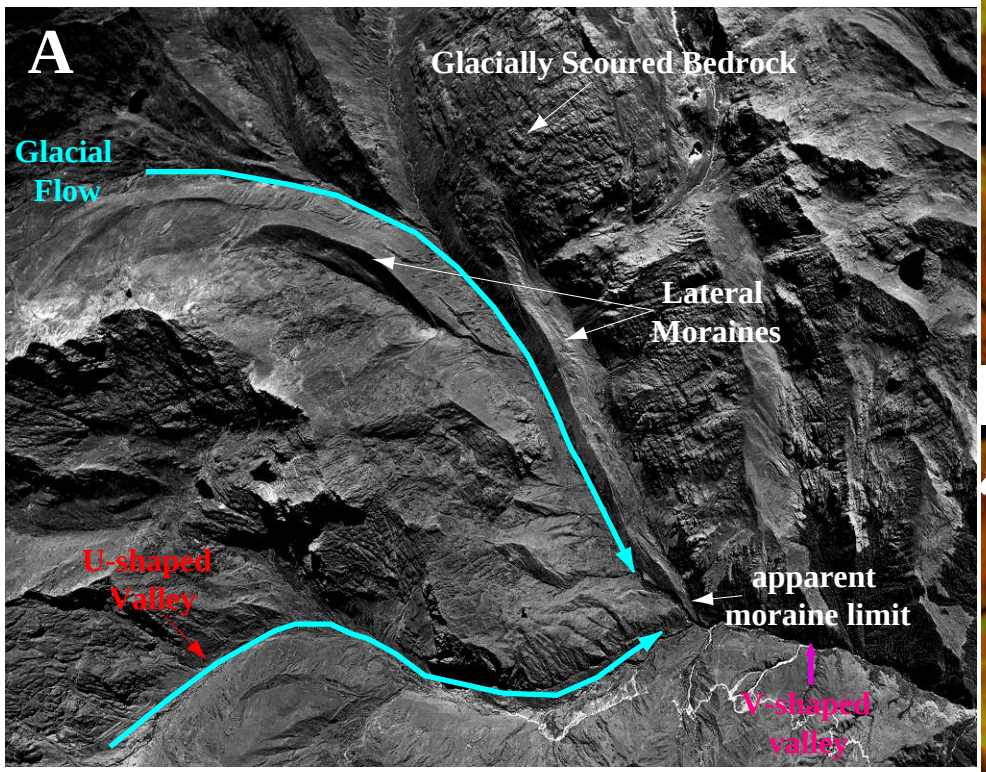

Approximate Scale

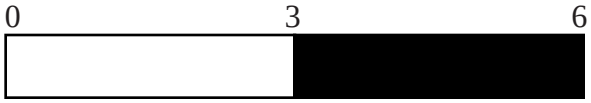

Landsat Thematic Mapper
(path 001 71)

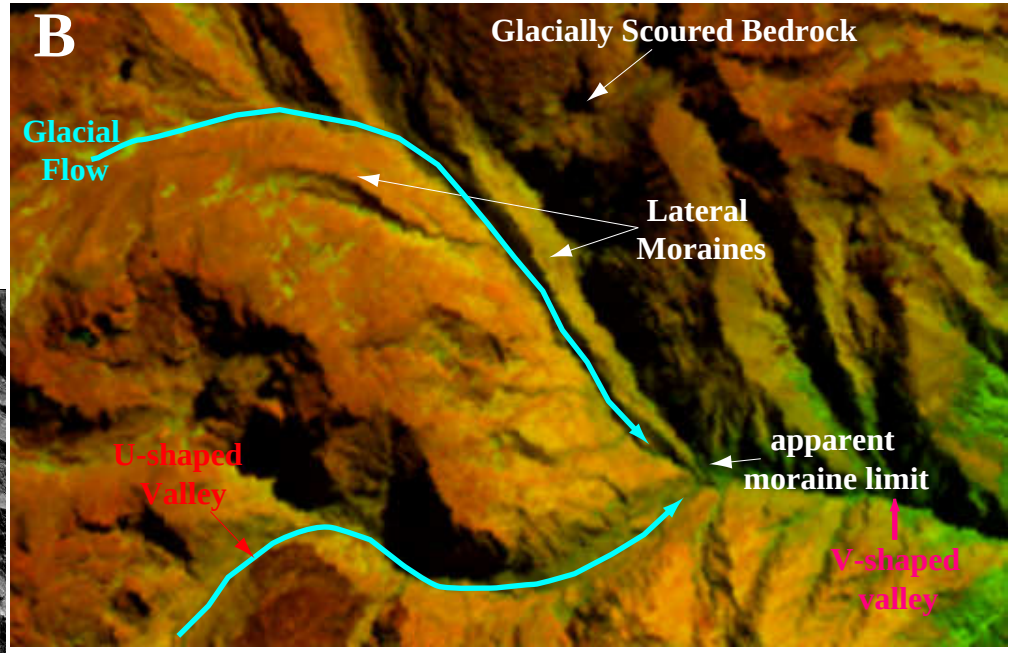

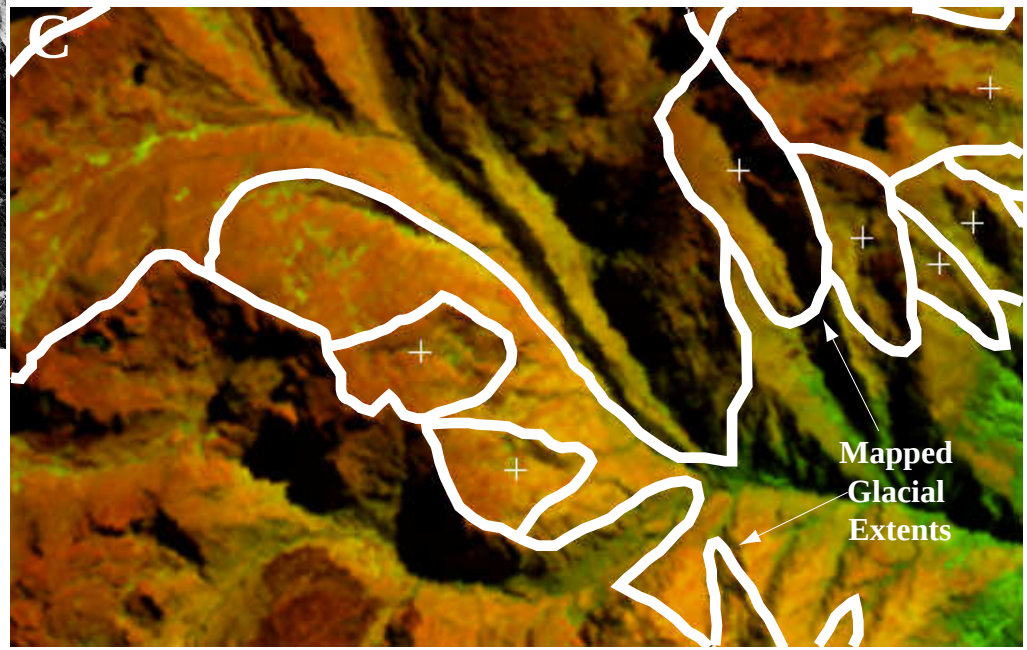

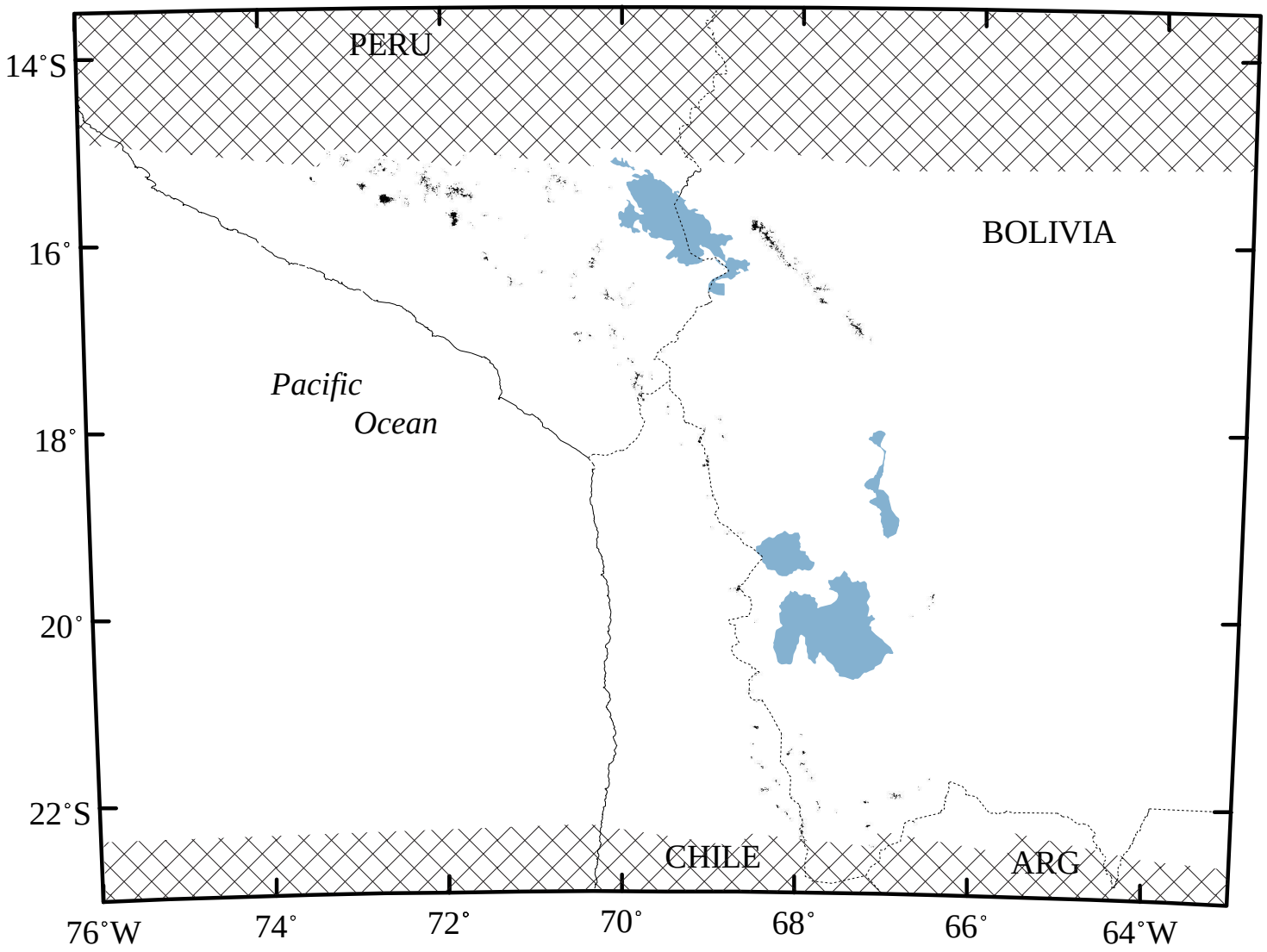
PERU
BOLIVIA
Pacific
Ocean
CHILE
ARG
14˚S
16˚
18˚
20˚
22˚S
76˚W
74˚
72˚
70˚
68˚
66˚
64˚W

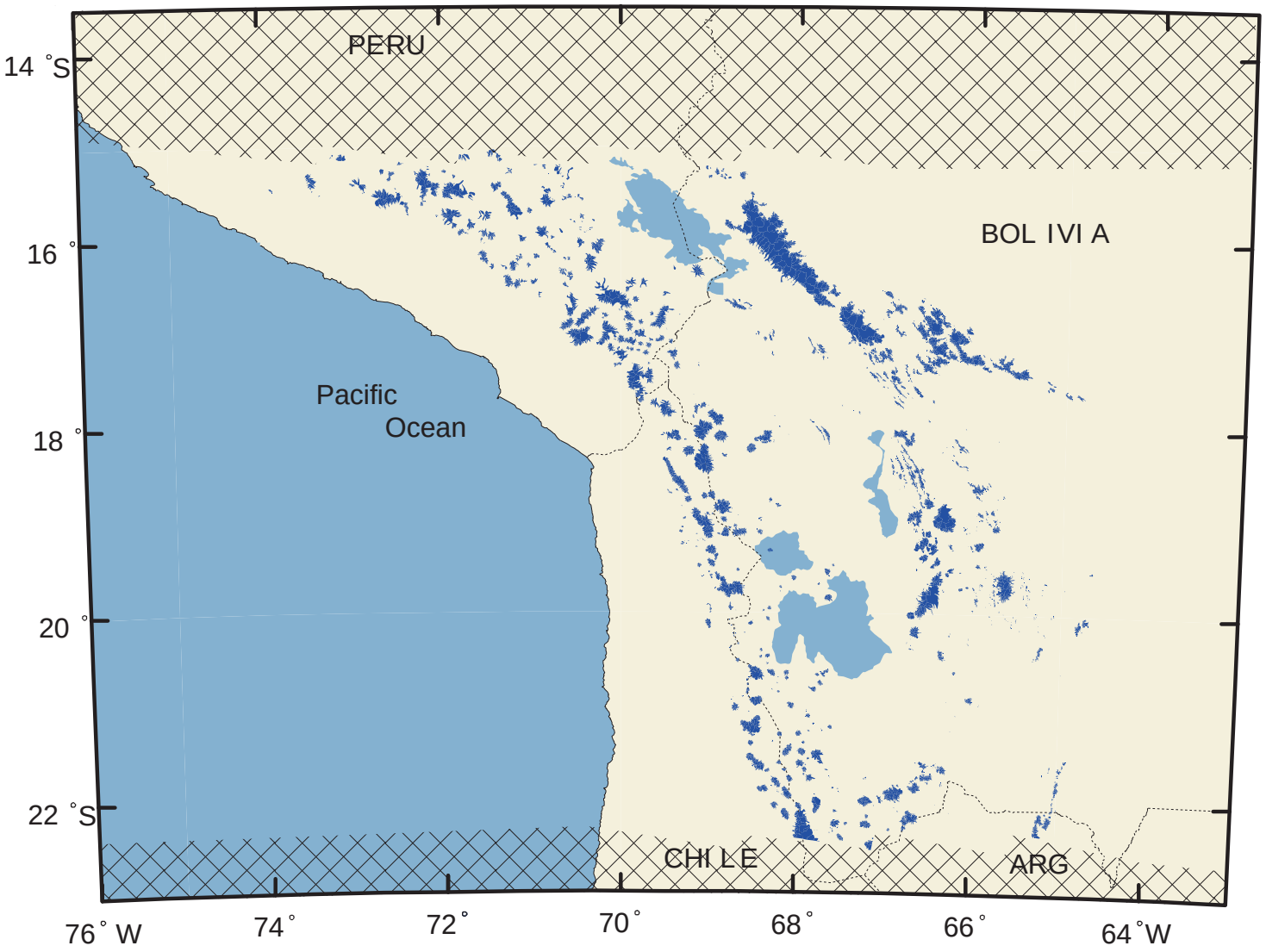
PERU
BOL IVI A
Pacific
Ocean
CHI L E
ARG
14 ˚S
16 ˚
18 ˚
20 ˚
22 ˚S
76 ˚ W
74 ˚
72 ˚
70 ˚
68 ˚
66 ˚
64 ˚W

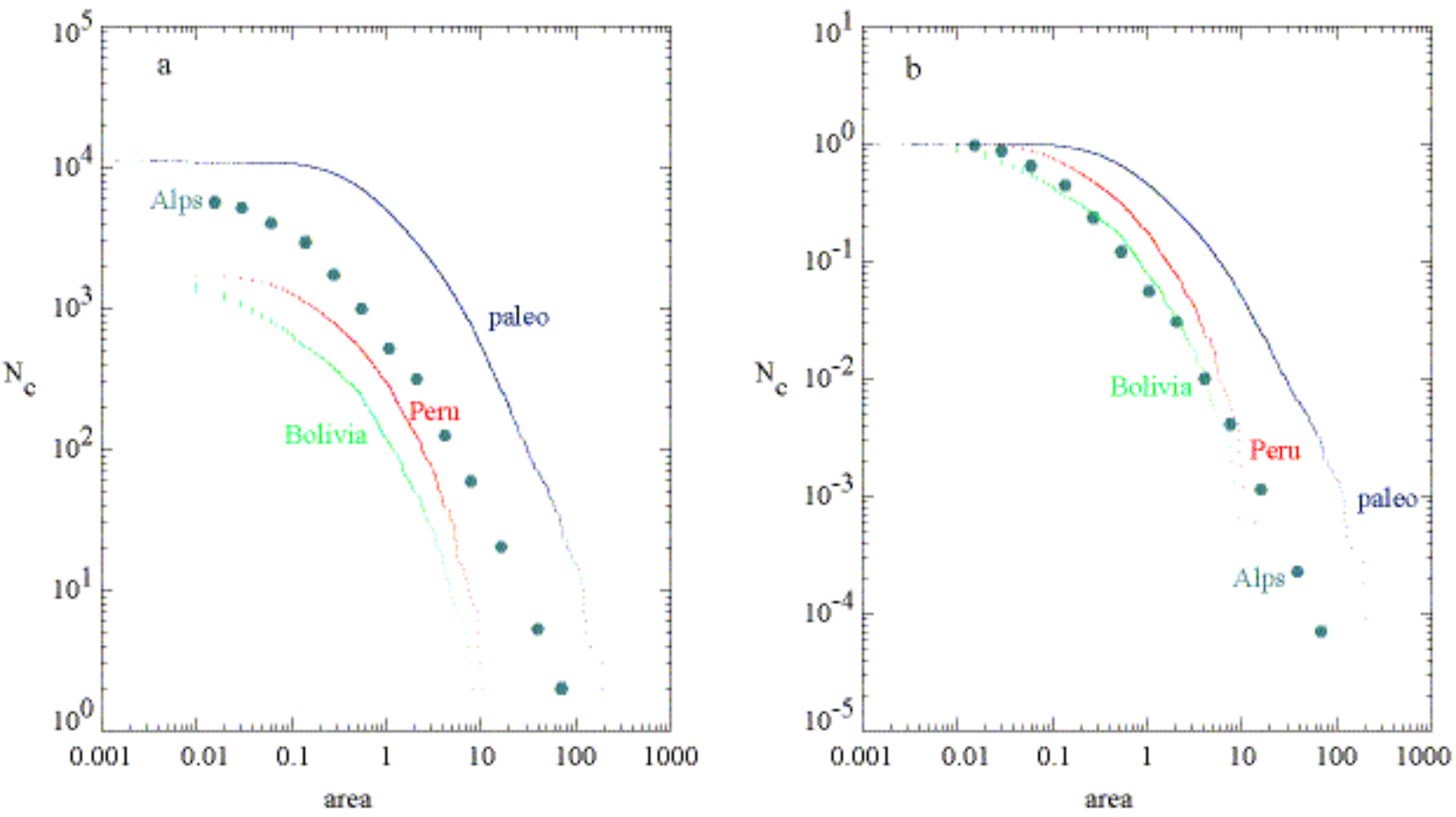
a
b
Alps
Bolivia
Peru
paleo
N_c
area
10^5
10^4
10^3
10^2
10^1
10^0
10^1
10^0
10^{-1}
10^{-2}
10^{-3}
10^{-4}
10^{-5}
0.001
0.01
0.1
1
10
100
1000

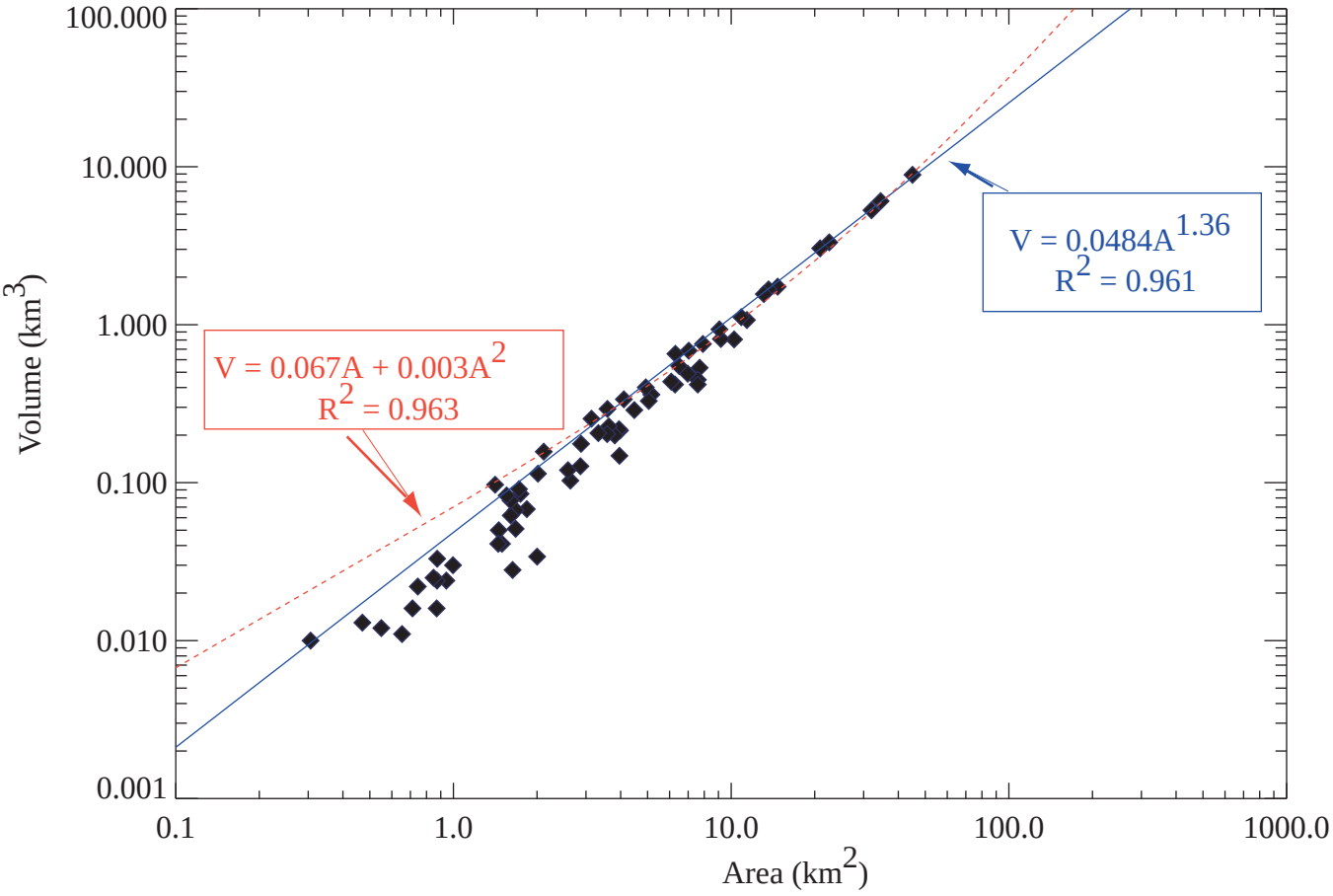
100.000
10.000
1.000
0.100
0.010
0.001
Volume (km3)
0.1
1.0
10.0
100.0
1000.0
Area (km2)
V = 0.067A + 0.003A2
R2 = 0.963
V = 0.0484A1.36
R2 = 0.961

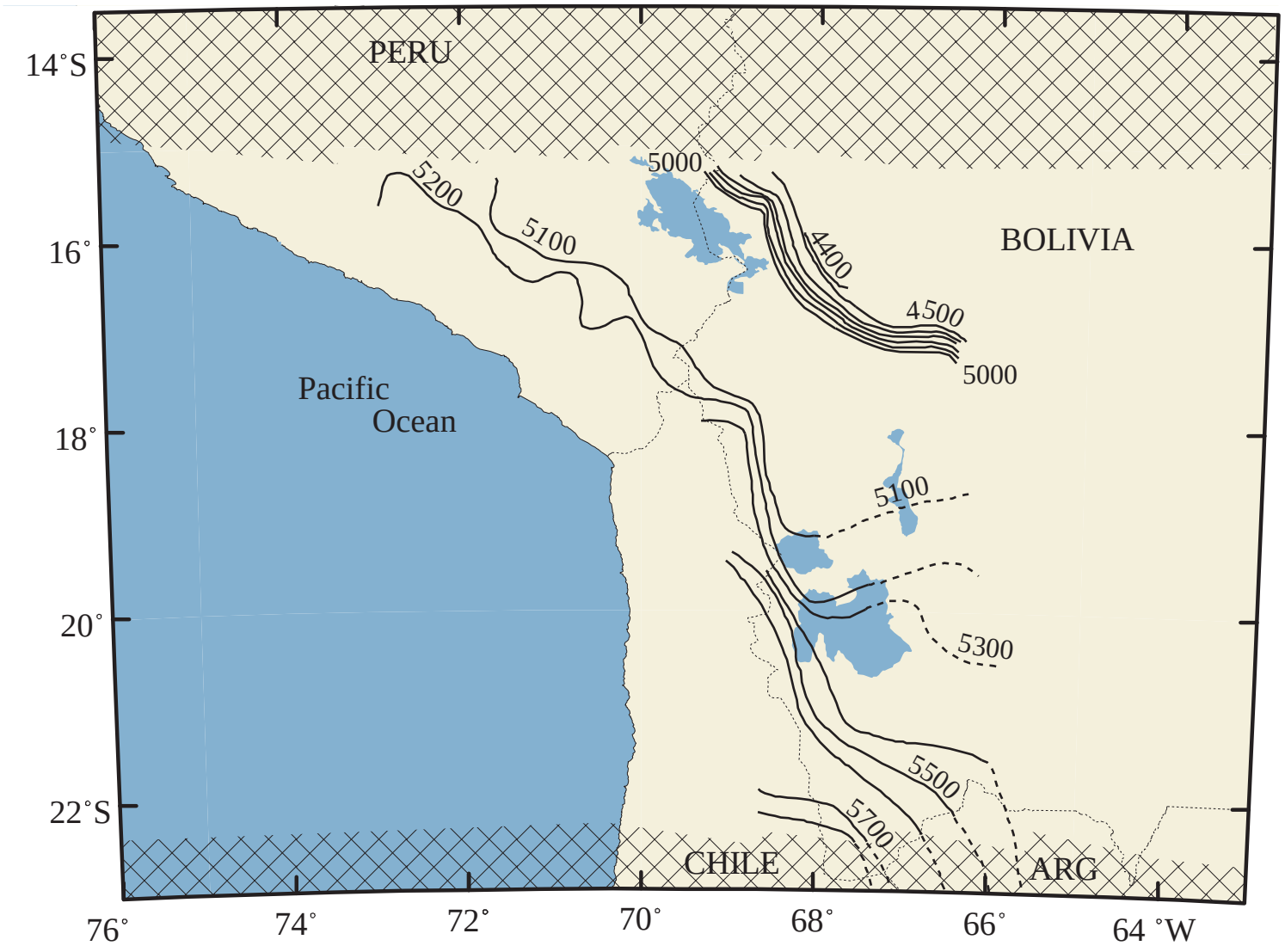
PERU
BOLIVIA
Pacific
Ocean
CHILE
ARG
5000
5200
5100
4400
4500
5000
5100
5300
5500
5700
14˚S
16˚
18˚
20˚
22˚S
76˚
74˚
72˚
70˚
68˚
66˚
64 ˚W

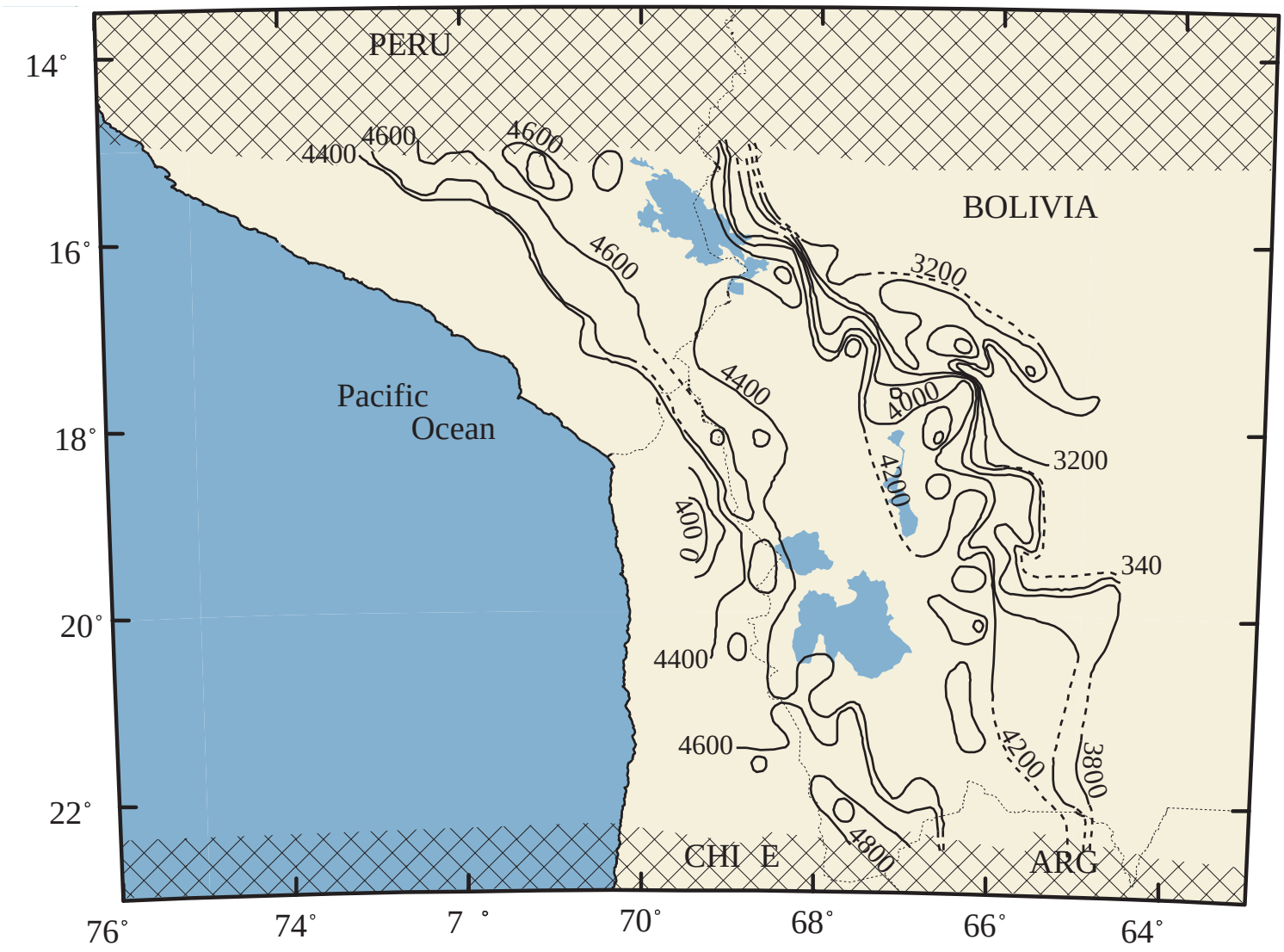
PERU
BOLIVIA
Pacific
Ocean
CHI E
ARG
14˚
16˚
18˚
20˚
22˚
76˚
74˚
7 ˚
70˚
68˚
66˚
64˚
4400
4600
4600
4600
4400
4000
4200
4000
3200
3200
340
4400
4600
4200
3800
4800

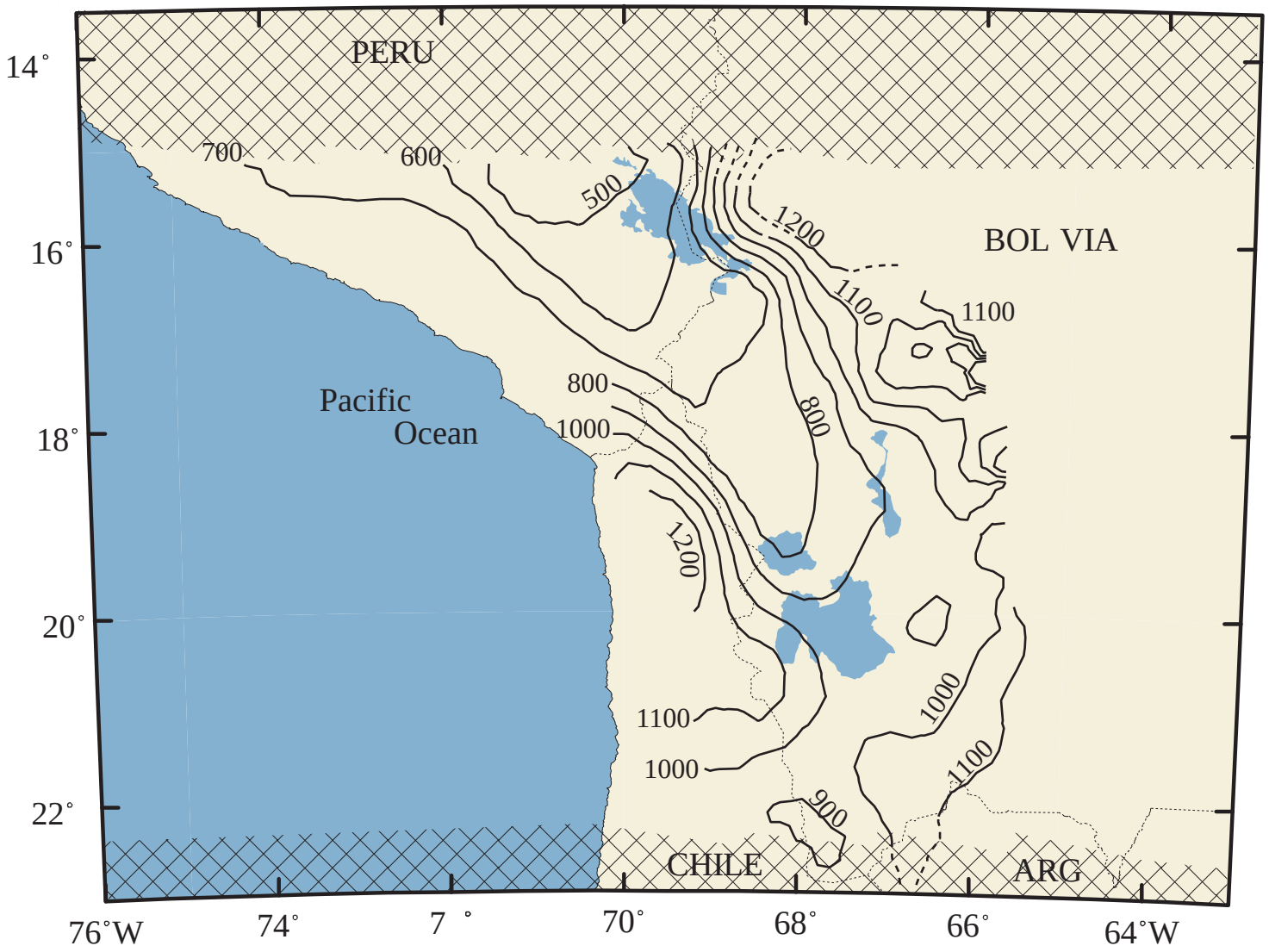
PERU
BOL VIA
CHILE
ARG
Pacific
Ocean
700
600
500
1200
1100
1100
800
1000
800
1200
1100
1000
1000
1100
900
14˚
16˚
18˚
20˚
22˚
76˚W
74˚
7 ˚
70˚
68˚
66˚
64˚W